Defect states and excitations in a Mott insulator with orbital degrees of freedom: Mott-Hubbard gap versus optical and transport gaps in doped systems

Adolfo Avella,[1,2,3,4] Peter Horsch,[1] and Andrzej M. Oleś[1,5]

[1]*Max-Planck-Institut für Festkörperforschung, Heisenbergstrasse 1, D-70569 Stuttgart, Germany*

[2]*Dipartimento di Fisica "E.R. Caianiello," Università degli Studi di Salerno, I-84084 Fisciano (SA), Italy*

[3]*CNR-SPIN, UoS di Salerno, I-84084 Fisciano (SA), Italy*

[4]*Unità CNISM di Salerno, Università degli Studi di Salerno, I-84084 Fisciano (SA), Italy*

[5]*Marian Smoluchowski Institute of Physics, Jagellonian University, Reymonta 4, PL-30059 Kraków, Poland*

(Received 26 October 2012; published 31 January 2013)

We address the role played by charged defects in doped Mott insulators with active orbital degrees of freedom. It is observed that defects feature a rather complex and rich physics, which is well captured by a degenerate Hubbard model extended by terms that describe crystal-field splittings and orbital-lattice coupling, as well as by terms generated by defects such as the Coulomb potential terms that act both on doped holes and on electrons within occupied orbitals at undoped sites. We show that the multiplet structure of the excited states generated in such systems by strong electron interactions is well described within the unrestricted Hartree-Fock approximation, once the symmetry breaking caused by the onset of magnetic and orbital order is taken into account. Furthermore, we uncover spectral features that arise within the Mott-Hubbard gap and in the multiplet spectrum at high energies due to the presence of defect states and strong correlations. These features reflect the action on electrons/holes of the generalized defect potential that affects charge and orbital degrees of freedom, and indirectly also spin ones. This study elucidates the mechanism behind the Coulomb gap appearing in the band of defect states and investigates the dependence on the electron-electron interactions and the screening by the orbital-polarization field. As an illustrative example of our general approach, we present explicit calculations for the model describing three t_{2g} orbital flavors in the perovskite vanadates doped by divalent Sr or Ca ions, such as in $La_{1-x}Sr_xVO_3$ and $Y_{1-x}Ca_xVO_3$ systems. We analyze the orbital densities at vanadium ions in the vicinity of defects and the excited defect states which determine the optical and transport gaps in doped systems.

DOI: 10.1103/PhysRevB.87.045132 PACS number(s): 71.55.−i, 71.10.Fd, 75.25.Dk, 78.20.Bh

I. INTRODUCTION

Doped vanadium perovskites show a very rich behavior that has been mainly explored by experimentalists during the last decade.[1–8] In contrast to the high-T_c cuprates,[9–14] the perovskite vanadates represent quite generally systems with an active orbital degree of freedom.[15–18] The particular excitement with the RVO_3 perovskite mother compounds, where $R =$ Lu, Yb, ..., La, is the quantum interplay of spin-orbital degrees of freedom,[19–28] which is only under partial control of weak Jahn-Teller (JT) and other couplings.[29] The moderate coupling to the lattice results from the t_{2g} character of the outer valence electrons[30] and explains that the orbital quantum dynamics is not quenched, a property vanadates share with other transition-metal oxides such as, for example, titanates[31,32] and iridates.[33,34] The phase diagrams of doped vanadates[3] deduced from the resistivity, specific heat, and magnetic measurements show a systematic decrease of magnetic interactions and the onset of the metallic behavior only at rather high doping,[3] in contrast, for instance, to the high-T_c cuprates where the metal-insulator transition (MIT) is found at a few percent of hole doping.[35] In $La_{1-x}Sr_xVO_3$, perhaps the most investigated doped vanadium oxide, the MIT is at $x \simeq 0.18$ Sr doping,[2] while $Y_{1-x}Ca_xVO_3$ is insulating up to $x \simeq 0.50$.[4] This latter compound undergoes a transition from the GC phase to the CG phase[36] at rather low doping $x \sim 0.02$ within the insulating phase. It was pointed out[23] that the double exchange[37–40] is the mechanism responsible for this transition in antiferromagnetic (AF) phases, similar to the transition from the G-type AF (G-AF) to C-type AF (C-AF) order in electron-doped manganites.[41] In addition, the change of superexchange interaction in the vicinity of the holes[42] bound to the defects has a strong influence on the relative energy of these states.[43] Remarkably, the CG spin-orbital order persists up to the MIT.

The evolution of optical spectra with doping for these two vanadium perovskites,[4] $La_{1-x}Sr_xVO_3$ and $Y_{1-x}Ca_xVO_3$, shows that the defects lead to impurity states which are responsible for an absorption band deep inside the Mott-Hubbard (MH) gap.[43] This suggests that bound small polarons are the cause of the MIT even at high doping concentrations.[4] It is eventually the growth of the mid-infrared absorption under increasing doping and the gradual shift of this absorption toward zero energy, which accompanies the MIT. These experimental findings call for a theoretical approach that would address the nature of defects and the changes in the magnetic and orbital structure induced by them in a Mott insulator. Doping in combination with strong correlations leads to spectral weight transfer,[43] while on the other hand, the size of the MH gap is not significantly influenced by doping.[4] We discuss these issues in this paper and point out that the defect states here should be distinguished from those observed within the MH gap in other circumstances such as the excitonic states in $LiCuVO_4$,[44] or the states generated simply by doping an orbitally ordered Mott insulator in absence of defects.[45]

The description of defect states in systems with strongly correlated electrons is an outstanding problem in the theory of condensed matter,[46] and has been addressed mainly within the Hartree-Fock (HF) approach[43,47–49] and the methods based

on density functional theory.[50–52] It involves, for example, questions such as the following: (i) What is the nature of defect states in a strongly correlated system, i.e., as compared to defects in usual semiconductors or insulators?[53–55] (ii) What happens to the MH gap in the presence of defects? (iii) Which are the new features in orbital degenerate MH insulators as, for example, in the t_{2g} transition-metal oxides with active orbital degree of freedom, in contrast to doped high-T_c superconductors? (iv) Which are practicable methods to perform reliable calculations for MH insulators that can be extended to take into account defects and disorder? The answer to all these questions is a formidable challenge as the defects may strongly affect the subtle interplay of several essential degrees of freedom, namely, spin, orbital, lattice, and charge, as we shall see in the following.

It is remarkable that the theoretical analysis of doping in transition-metal oxides, including manganites and also superconducting cuprates, is usually performed in the metallic regime where the effect of doping on the properties of a material with strongly correlated electrons leads solely to the modification of the electronic filling in party filled $3d$ orbitals.[15] This simplification is not possible in the insulating regime where local defect fields are not screened, leading to defect states as, for example, in the case of Ca defects in the lattice of Y ions in $Y_{1-x}Ca_xVO_3$.[43] Here, we explore further this idea and analyze a model with three t_{2g} orbital flavors. This is a generalization of the frequently used two-flavor model (with active $\{xz, yz\}$ orbitals) for $R\mathrm{VO}_3$ compounds,[19–23,25,26,43] motivated by earlier electronic-structure studies.[56–58] The first electron at each V^{3+} ion occupies the xy orbital, with energy lowered by the crystal field, while the second one occupies one of two degenerate orbitals, either the yz or xz, resulting in an $xy^1(yz/zx)^1$ local configuration.

The purpose of this paper is to introduce a systematic unbiased approach that allows one to study defect states in strongly correlated materials. As we show in the following, the interactions, which arise by introducing charged defects into a Mott insulator, are numerous and all of them are necessary in a realistic approach that is capable of predicting experimental behavior of a doped material. We adopt here a multiband Hubbard model[59] that is supplemented by several terms responsible for the influence of the lattice and defect states on the electronic structure. We use it below for the description of t_{2g} electrons and generalize thereby earlier approaches.[17,60,61] The electronic structure will be analyzed using the unrestricted HF approximation,[62–64] which is known to be reliable in systems with spontaneously broken symmetry, for instance, for states wth magnetic order in multiband models for manganites,[47] CuO_2 planes in high temperature superconductors,[65] and low-dimensional cuprates,[66] and may also serve to describe complex types of order such as stripe or spiral structures.[67–69] As we demonstrate in the following, charged defects are the source of impurity states which appear as new features within the MH gap, while the MH gap itself is essentially unaffected in the low-doping regime.[4] Hence, the defect states are responsible for the in-gap absorption in the optical conductivity at low doping. At the same time, we demonstrate that the HF method used here is well designed to treat simultaneously phenomena that arise at distinct energy scales, the high energy $\sim$1 eV related to the (onsite and intersite) Coulomb interaction around the defect states and the low-energy scale $\sim$0.1 eV that is related to the orbital physics and controls electronic transport in doped materials.

The problem addressed here pertains to general transition-metal oxides with perovskite or layered structure, which feature a variety of interesting phenomena due to strong electron correlations. They include MITs in undoped systems, several phenomena with long-range (LR) coherence in doped systems, such as high-T_c superconductivity,[10–14] colossal magnetoresistance, phases with magnetic and orbital order, and so on. In particular, the doped manganese oxides with colossal magnetoresistance show several magnetic phase transitions[70–72] that have attracted a broad interest in the interplay between spin, orbital, and charge degrees of freedom in strongly correlated electron systems. In this class of systems, orbitals couple strongly to the lattice, and this coupling supports the superexchange,[73] leading to well-separated energy scales for the structural and magnetic transition.[72] In contrast, the $R\mathrm{VO}_3$ perovskites are a challenge for the theory of spin-orbital systems as the magnetic and orbital orders occur here in the same range of temperatures, or even simultaneously as in $LaVO_3$.[6,74]

A common feature of the $R\mathrm{VO}_3$ perovskites is the onset of the G-type alternating orbital (G-AO) order below the characteristic orbital ordering temperature T_{OO}, which is in these compounds relatively low, $T_{\mathrm{OO}} \simeq 200$ K, and exhibits nonmonotonous dependence on the ionic radius of R ions.[6,74] The temperature T_{OO} comes close to the Néel temperature $100 < T_{\mathrm{N1}} < 140$ K for the magnetic transition to the C-type antiferromagnetic (C-AF) phase. This phase competes with another AF phase in the $R\mathrm{VO}_3$ systems with small radii of R ions.[6] In such cases, this latter GC phase is stable at low temperature, while the former CG phase takes over when temperature increases. The best-known example of this behavior is YVO_3 with a transition temperature $T_{\mathrm{N2}} = 77$ K. It has been shown in Ref. 21 that relativistic spin-orbit interaction is important to describe the reorientation of spins associated with the two different types of order at this first-order phase transition. A remarkable reversal of the magnetization direction[75,76] inside the CG phase with increasing temperature could not be understood in the theory until now.

The principal difficulty in the theory of the $R\mathrm{VO}_3$ perovskites is the quantum interplay of spin-orbital degrees of freedom,[19] which manifests itself in leading contributions that emerge due to spin-orbital entanglement.[24,28] Quantum effects associated with joint spin-orbital dynamics play a role at zero and at finite temperatures[77–79] and the consequences have been observed in several experiments[28]: (i) the temperature dependence of the optical spectral weights,[77] (ii) the apparent breakdown of Goodenough-Kanamori rules for magnetic interactions in the CG phase [unlike in other orbitally degenerate systems, ferromagnetic (FM) interactions are here stronger than the AF ones],[78] (iii) the orbital-Peierls dimerization of FM interactions in the C-AF phase[20,21,27] observed in the neutron scattering in YVO_3,[78] and also in $LaVO_3$,[79] as well as (iv) the interplay between the spin and orbital correlations, which lead to the phase diagram of the $R\mathrm{VO}_3$ perovskites.[6] The Peierls instability of FM chains towards dimerization occurs when spin and orbital degrees of freedom are entangled at finite temperature,[27] and a previous theoretical study showed that charged defects favor orbital-Peierls dimerization in the small

doping regime.[43] Furthermore, orbital fluctuations and their competition with orbital-lattice coupling play a crucial role for the explanation of the observed nonmonotonous dependence of the orbital transition temperature on the radius r_R of R ions along the $R\mathrm{VO_3}$ series.[26] Other studies support the picture of strong orbital fluctuations and their decisive impact on the observed physical properties.[80–83] We show in the following that in spite of the above quantum nature of the spin-orbital order in the $R\mathrm{VO_3}$ perovskites, the HF approach is well designed to capture the essential features of charge defects.

The paper is organized as follows. First, in Sec. II A, we introduce a degenerate Hubbard model for t_{2g} electrons in the $R\mathrm{VO_3}$ perovskites and generalize it to the doped materials, such as $\mathrm{Y_{1-x}Ca_xVO_3}$ with $\mathrm{Ca^{2+}}$ charge defects replacing some $\mathrm{Y^{3+}}$ ions. The model includes local and intersite Coulomb interactions, and the Coulomb potentials induced by Ca defect states, which change locally the electronic structure of t_{2g} electrons within V($3d$) orbitals. We describe the treatment of this model in the unrestricted HF approximation in Sec. II B. In Sec. II C, we present the electronic structure obtained for the undoped CG and GC phases in Mott insulators for the typical parameters of $R\mathrm{VO_3}$. As explained there, the electronic structures provide a realistic description and include the multiplet structure of d^3 excited states. The optimized t_{2g} orbitals, at a vanadium ion being the nearest neighbor of a Ca defect, change to a new orthogonal basis due to the defect-orbital-polarization interaction, as shown in Sec. III. Next, we analyze the electron distribution on a bond next to a Ca defect in the CG and GC phases in Sec. IV A, and compare the unrestricted HF approach with the exact diagonalization (ED). We also analyze one-particle local charge excitations in Sec. IV B and demonstrate that their energies are well reproduced around the defect states when the intratomic Coulomb interaction U increases (see Sec. IV C). Next, we consider the electronic structure for the defect states in the CG phase in the dilute doping limit in Sec. V A, and introduce in Sec. V B the *order-parameter landscape* in a doped system. We study the effects of a finite orbital polarization in Sec. V C and investigate the changes induced by longer-range Coulomb interactions in Sec. V D.

This analysis is followed by the discussion of the electronic structure in a correlated material with defect states, where we address the gaps observed in the optical spectroscopy in Sec. VI A and the dependence of the electron density in xy orbitals on the defect concentration in Sec. VI B. Finally, the paper is summarized in Sec. VII, where we also present an outlook at possible future applications of the general unrestricted HF method introduced in the paper in doped transition-metal oxides. The Appendix highlights the importance of Fock terms in the present problem and addresses the concept of optimized orbitals in the vicinity of a charge defect.

II. MOTT INSULATOR WITH DEFECT STATES

A. Degenerate Hubbard model for t_{2g} electrons

We begin with introducing the multiband Hubbard model for t_{2g} electrons designed to describe doped $R\mathrm{VO_3}$ perovskites, such as the $\mathrm{Y_{1-x}Ca_xVO_3}$ compounds. This effective model includes only t_{2g} orbitals at vanadium ions $\mathrm{V^{3+}}$, coupled by effective d-d hopping elements along V–O–V bonds. Below, we consider how this picture is modified in presence of charged defects and, in particular, when not only the electron density within the t_{2g} orbitals of vanadium ions changes, but also the presence of Ca defects introduces local interactions acting on t_{2g} electrons at vanadium ions in their vicinity.

The multiband Hamiltonian that describes the MH physics of quasidegenerate t_{2g} electrons and the perturbations by the defect potentials consists quite generally of one-electron terms $\mathcal{H}_0$ and two-electron (Coulomb and JT) interactions $\mathcal{H}_{\rm int}$:

$$\mathcal{H} = \mathcal{H}_0 + \mathcal{H}_{\rm int}, \tag{2.1}$$

$$\mathcal{H}_0 = H_t + H_{\rm CF} + H_{\rm def}, \tag{2.2}$$

$$\mathcal{H}_{\rm int} = H_U + H_V + H_{\rm JT}. \tag{2.3}$$

The one-electron part (2.2) is composed of the following terms: (i) the kinetic energy (H_t), (ii) crystal-field (CF) splitting ($H_{\rm CF}$), and (iii) the perturbations generated by defects ($H_{\rm def}$). Here, $H_{\rm def}$ includes two terms:

$$\mathcal{H}_{\rm def} = H_{\rm imp} + H_{\rm pol}, \tag{2.4}$$

the Coulomb potentials of the charged impurities $H_{\rm imp}$ and the orbital-polarization term $H_{\rm pol}$. These two terms arise due to the presence of Ca defects, and they constitute effective fields that act on the vanadium ions in the neighborhood of defects. They have been introduced in a simplified (two-flavor) model with two active t_{2g} orbital flavors $\{yz,zx\}$ (Ref. 43) (see following).

The electron interactions $\mathcal{H}_{\rm int}$ (2.3) are given by (i) local Coulomb interactions (H_U), (ii) intersite Coulomb interactions (H_V), and (iii) the JT effective interactions between orbitals which are induced by lattice distortions ($H_{\rm JT}$). In the case of $R\mathrm{VO_3}$ perovskites considered here, the local Coulomb interactions are quite strong and lead to a Mott insulator with high spin ($S = 1$) and orbital degrees of freedom.[19,22] Depending on the parameters, the interactions in $\mathcal{H}_{\rm int}$ support a particular type of symmetry-broken phase,[25] and one expects coexisting spin and orbital order, either in the form of the CG or GC phase, in agreement with experimental observations.[6]

The kinetic energy describes the hopping processes between nearest-neighbor $\mathrm{V^{3+}}$ sites on bonds $\langle ij\rangle$ oriented along one of three cubic directions $\gamma = a,b,c$ in the perovskite lattice

$$H_t = \sum_{\langle ij\rangle\|\gamma}\sum_{\alpha,\beta,\sigma} t^{\gamma}_{\alpha\beta}(c^{\dagger}_{i\alpha\sigma}c_{j\beta\sigma} + c^{\dagger}_{j\beta\sigma}c_{i\alpha\sigma}). \tag{2.5}$$

Here, $c^{\dagger}_{i\alpha\sigma}$ is the electron creation operator at the $\mathrm{V^{3+}}$ ion at site i, with orbital flavor α and spin $\sigma = \uparrow,\downarrow$. The summation runs over all bonds $\langle ij\rangle\|\gamma$. The effective hopping t originates from two subsequent d-p hopping processes via the intermediate O($2p_\pi$) orbital along each V–O–V bond. It follows from the charge-transfer model with p-d hybridization t_{pd} and charge-transfer energy Δ (Ref. 30) that t is finite only between two identical t_{2g} orbitals, labeled $\alpha(\gamma)$, that are active along a given bond $\langle ij\rangle\|\gamma$. The third orbital, which lies in the plane perpendicular to the γ axis, is inactive as the hopping processes vanish here by symmetry. This motivates the convenient notation used hereafter[19]

$$|a\rangle \equiv |yz\rangle, \quad |b\rangle \equiv |xz\rangle, \quad |c\rangle \equiv |xy\rangle, \tag{2.6}$$

where the orbital $|\gamma\rangle$ inactive along a cubic direction γ is labeled by its index. Thus, if we consider an idealized case

without lattice distortions and without defects, the hopping conserves the t_{2g} orbital flavor

$$t^{\gamma}_{\alpha\beta} = -t\delta_{\alpha\beta}(1-\delta_{\gamma\alpha}). \tag{2.7}$$

Using the charge-transfer model,[30] one estimates the hopping element $t = t^2_{pd}/\Delta \simeq 0.2$ eV; this value appears to be consistent with that deduced from the electronic-structure calculations.[58]

The t_{2g} orbital states are nonequivalent in the RVO$_3$ perovskites due to the GdFeO$_3$-like distortions,[84] and one finds that the c orbitals are occupied at every site. This is a consequence of the CF splitting term [see Eq. (2.1)], which favors c orbital occupation

$$H_{\rm CF} = -\varepsilon^0_c \sum_i n_{ic}\,, \tag{2.8}$$

where $n_{i\alpha} = \sum_\sigma n_{i\alpha\sigma}$, with $n_{i\alpha\sigma} = c^\dagger_{i\alpha\sigma}c_{i\alpha\sigma}$, is the electron density operator for spin orbital $\{\alpha\sigma\}$ at site i. We estimated[26] $\varepsilon^0_c \sim t$, hence, the c orbital is filled by one electron and the second electron at any V^{3+} ion occupies one of the orbitals in the $\{a,b\}$ doublet, leading to a $c^1_i(a,b)^1_i$ configuration at each site i. This broken-symmetry state, which corresponds to electron densities

$$\langle n_{ic}\rangle = 1, \quad \langle n_{ia}+n_{ib}\rangle = 1, \tag{2.9}$$

within t_{2g} orbitals at undoped V^{3+} ions, is stable in a Mott insulator even for values of ε_c as small as $0.5t$ and justifies the two-flavor model.[43] Note, however, that one expects that the cubic symmetry with $n_{i\gamma} = \frac{2}{3}$ is restored at high temperatures,[19,25] but this situation will not be analyzed here.

The defect terms in H_0 [Eq. (2.2)] describe Coulomb interactions of the charged defects and the t_{2g} electrons within orbitals at neighboring vanadium ions and act on them as effective fields. As explained elsewhere,[43] when an Y^{3+} ion in YVO$_3$ is replaced by a Ca^{2+} impurity in the doped compound Y$_{1-x}$Ca$_x$VO$_3$, the lattice is locally disturbed and the impurity acts as an effective *negative charge* in the sublattice of Y ions: it is located in the center of the V$_8$ cube surrounding the defect site (see Fig. 1 of Ref. 43). Such a defect is therefore responsible for additional Coulomb interaction terms between the impurity charge and the electron charges in t_{2g} orbitals of surrounding vanadium ions. The first additional term is the Coulomb potential due to the Ca impurity $H_{\rm imp}$, which describes the Coulomb interaction between the defect at site m with effective negative charge $Q_m = e$ (here we adopt $e = 1$) and the total t_{2g} electron charge density operator at the V ion at site i:

$$H_{\rm imp} = \sum_{\mathbf{m}\in\mathcal{D}}\sum_i W(|\mathbf{r}_i - \mathbf{R}_m|)\, n_i\,, \tag{2.10}$$

where $n_i = \sum_\alpha n_{i\alpha}$ is the electron density operator. Here, the first sum runs over the Ca defects labeled with $m \in \mathcal{D}$, where the set $\mathcal{D}$ contains all lattice defect sites at the considered doping x in Y$_{1-x}$Ca$_x$VO$_3$. The second index i labels V ions at distance $|\mathbf{r}_i - \mathbf{R}_m|$ from the considered defect site m. In general, the coordinates of the defects $\{\mathbf{R}_m\}$ are statistically distributed, although defects will also feel some repulsion that avoids their clustering. The defect potential of an impurity with negative charge $Q_D = e$ is of Coulomb type $W(r) = eQ_D/\epsilon_c r$, where ϵ_c is the dielectric constant (of core electrons).[43] Following, we shall employ a truncated defect potential

$$W(|\mathbf{r}_i - \mathbf{R}_m|) = \begin{cases} V_D & \text{if } i \in \mathcal{C}^1_m, \\ 0 & \text{otherwise,} \end{cases} \tag{2.11}$$

i.e., i should belong to the V$_8$ cube $\mathcal{C}^1_m \equiv \mathcal{C}^1(\mathbf{R}_m)$ formed by eight nearest-neighbor V sites surrounding the Ca defect at site m (V$_8$ cube). With a dielectric constant $\epsilon_c \simeq 5$ for YVO$_3$, one finds for the defect potential $V_D \simeq 1$ eV.[43] We note that the truncated potential is introduced here as it provides later on a more transparent interpretation of the spectra and facilitates the analysis of the energy shifts of defect states.

The last term in Eq. (2.2) is the orbital-polarization term $H_{\rm pol}$. The V ions surround a defect site and form a V$_8$ cube,[43] occupying the positions shown in Fig. 1(a). $H_{\rm pol}$ originates from the quadrupolar component of electrostatic field generated by a charge defect within the lattice of V^{3+} ions. At each vanadium ion, the Coulomb repulsion between the defect charge and t_{2g} electrons favors the occupation of the linear combinations of t_{2g} orbitals that maximize the average distance of the electronic charge from the defect.

Consequently, the defect-orbital interaction, called below orbital polarization, takes the form

$$H_{\rm pol} = D\sum_{\mathbf{m}\in\mathcal{D}}\sum_{\substack{i\in\mathcal{C}_m \\ \alpha\neq\beta}} \lambda_{\alpha\beta}(\mathbf{r}_i - \mathbf{R}_m)(c^\dagger_{i\alpha\sigma}c_{i\beta\sigma} + c^\dagger_{i\beta\sigma}c_{i\alpha\sigma}). \tag{2.12}$$

The coefficients $\{\lambda_{\alpha\beta}(\mathbf{r}_i - \mathbf{R}_m)\} = \pm 1$ depend on the pair of considered orbitals $\alpha\beta$ and on the direction $\mathbf{r}_i - \mathbf{R}_m$; they are selected to minimize the Coulomb repulsion. This is achieved by

$$\lambda_{ab}(\mathbf{r}_i - \mathbf{R}_m) = \begin{cases} 1 & \text{if } \mathbf{r}_i - \mathbf{R}_m \parallel (111),(11\bar{1}), \\ -1 & \text{if } \mathbf{r}_i - \mathbf{R}_m \parallel (\bar{1}11),(1\bar{1}1), \end{cases} \tag{2.13}$$

$$\lambda_{ac}(\mathbf{r}_i - \mathbf{R}_m) = \begin{cases} 1 & \text{if } \mathbf{r}_i - \mathbf{R}_m \parallel (111),(\bar{1}11), \\ -1 & \text{if } \mathbf{r}_i - \mathbf{R}_m \parallel (1\bar{1}1),(11\bar{1}), \end{cases} \tag{2.14}$$

$$\lambda_{bc}(\mathbf{r}_i - \mathbf{R}_m) = \begin{cases} 1 & \text{if } \mathbf{r}_i - \mathbf{R}_m \parallel (111),(1\bar{1}1), \\ -1 & \text{if } \mathbf{r}_i - \mathbf{R}_m \parallel (\bar{1}11),(11\bar{1}). \end{cases} \tag{2.15}$$

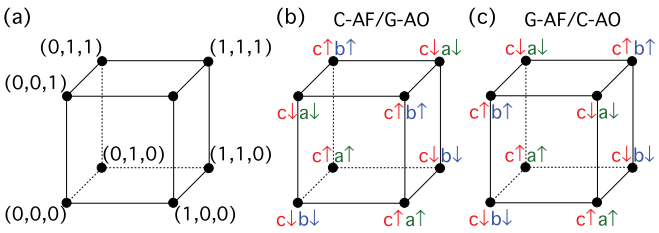

FIG. 1. (Color online) (a) Reference coordinates (klm) of vanadium ions in a representative V$_8$ cube in YVO$_3$. Phases with spin-orbital order of perovskite vanadates considered in this paper have the electron occupancies in the two magnetic phases shown schematically in (b) C-AF/G-AO phase; (c) G-AF/C-AO phase. The occupied orbitals $\{a,b,c\}$ and their spin components $\{\uparrow,\downarrow\}$ are indicated at each corner of the cube.

Note that each direction along one of the diagonals of the cube involves two vanadium ions.

The local Coulomb interactions between t_{2g} electrons at V^{3+} ions are described by[59]

$$H_U = U \sum_{i,\alpha} n_{i\alpha\uparrow} n_{i\alpha\downarrow} + \left(U - \frac{5}{2} J_H\right) \sum_{i,\alpha<\beta} n_{i\alpha} n_{i\beta} - 2J_H \sum_{i,\alpha<\beta} \mathbf{S}_{i\alpha} \cdot \mathbf{S}_{i\beta} + J_H \sum_{i,\alpha\neq\beta} c^{\dagger}_{i\alpha\uparrow} c^{\dagger}_{i\alpha\downarrow} c_{i\beta\downarrow} c_{i\beta\uparrow}. \tag{2.16}$$

Here, the spin operators for orbital α at site i, $\mathbf{S}_{i\alpha}$, are defined through the Pauli matrices $\{\sigma_x,\sigma_y,\sigma_z\}$ and are related to fermion operators in the standard way, i.e.,

$$S^{+}_{i\alpha} \equiv c^{\dagger}_{i\alpha\uparrow} c_{i\alpha\downarrow}\,, \quad S^{z}_{i\alpha} \equiv \tfrac{1}{2}(n_{i\alpha\uparrow} - n_{i\alpha\downarrow})\,. \tag{2.17}$$

The first term in Eq. (2.16) describes the intraorbital Coulomb interaction U between electrons with antiparallel spins; the second one stands for Hund's exchange J_H. These two parameters $\{U,J_H\}$ suffice to describe local Coulomb interactions between t_{2g} electrons considered here and are determined by the effective Racah parameters $\{A,B,C\}$;[85] the remaining terms are the interorbital Coulomb density-density interaction, and the so-called "pair-hopping" term which acts in the subspace of doubly occupied orbitals. The choice of coefficients in Eq. (2.16) guarantees that the interactions obey the rotational invariance in the orbital space.[59] Note that this Hamiltonian is exact when it describes only one representation of the cubic symmetry group (either t_{2g} or e_g) for $3d$ orbitals; this applies to the present case of partly occupied t_{2g} orbitals in the $R\mathrm{VO}_3$ perovskites. In general, however, the interorbital Coulomb and Hund's exchange interactions are both anisotropic,[17] and preserving rotational invariance requires also including onsite three-orbital and four-orbital terms; more details may be found in Refs. 85–88.

The LR Coulomb interaction has the usual expression

$$H_V = \frac{1}{2} \sum_{i\neq j,\alpha\beta} V_{ij} n_{i\alpha} n_{j\beta}, \tag{2.18}$$

where the Coulomb interaction V_{ij} is parametrized by the nearest-neighbor matrix element V_1:

$$V_{ij} = \frac{V_1}{|\mathbf{r}_i - \mathbf{r}_j|}\,, \tag{2.19}$$

with coordinates $\mathbf{r}_i = (i_a,i_b,i_c)$ and $\mathbf{r}_j = (j_a,j_b,j_c)$, respectively, given in integer representation. We assume that the interaction parameter V_1 accounts implicitly for the background dielectric function due to the core electrons. For convenience, we define the nearest-neighbor interaction

$$V_1 = \kappa V_{\mathrm{ee}}, \tag{2.20}$$

in terms of the electron-electron interaction strength V_{ee}, where the parameter $\kappa = \frac{\sqrt{3}}{2}$ represents the ratio d/a; here, a is the V-V lattice constant and d is the distance between the defect and the nearest V neighbor. In this paper, we discuss results obtained either without the intersite Coulomb interaction ($V_{\mathrm{ee}} = 0$) or with the full LR interaction.

The JT term $\mathcal{H}_{\mathrm{JT}}$ describes intersite orbital-orbital interactions that follow from lattice distortions and concern the orbital doublet $\{a,b\}$. The distortions are both of the JT type and $GdFeO_3$ type and jointly induce orbital alternation in the ab planes and favor identical orbitals along the c axis; these interactions are included here by the following expression:[19,43]

$$H_{\mathrm{JT}} = V_{ab} \sum_{\langle ij\rangle \| a,b} \tau^z_i \tau^z_j - V_c \sum_{\langle ij\rangle \| c} \tau^z_i \tau^z_j\,, \tag{2.21}$$

where

$$\tau^z_i \equiv \tfrac{1}{2}(n_{ia} - n_{ib}) \tag{2.22}$$

is the zth component of the orbital pseudospin $\tau = \frac{1}{2}$ along the c axis influenced by lattice distortions. The interaction parameters $V_{ab} > 0$ and $V_c > 0$ influence the subtle balance between the magnetic phases in the $R\mathrm{VO}_3$ perovskites,[6] supporting the C-AO order, as realized for instance in the undoped YVO_3 at low temperatures (in the GC phase). These interactions increase within the $R\mathrm{VO}_3$ perovskites towards the compounds with small ionic radii, and this dependence plays a crucial role in the detailed understanding of the phase diagram of these perovskites.[26]

B. Hartree-Fock approximation

The degenerate Hubbard Hamiltonian, introduced in the previous section to describe t_{2g} electrons in a system with charged defects, can be solved exactly by ED only for very small systems. We present such calculations for a single atom and for a bond in Secs. III and IV, respectively. Treatment of larger systems is possible only after introducing approximations, either in the strong-coupling regime, where charge degrees of freedom can be integrated out,[17,43] or using HF approximation. We adopt here the latter general approach, which requires the self-consistent calculation of the full density matrix. We performed calculations that describe $Y_{1-x}Ca_xVO_3$ compound in the regime of low doping using finite clusters with defects of size $N \times N \times N$, and implemented periodic boundary conditions (PBC). We present the results obtained for $N = 8$ in Secs. V and VI.

The main aim of this paper is to calculate the electronic structure of strongly correlated and doped MH insulators, i.e., including the defects with their complex structure. This implies a computational challenge due to the simultaneous appearance of the strong correlation problem and the perturbations introduced by defects into the electronic structure. Certainly, it requires reliable approximations to deal with strong correlations and disorder simultaneously. The HF approach is an efficient scheme which maps the interacting electron problem onto the problem of a single particle moving in a self-consistently determined field that stems from all other electrons. Whether the HF approach is indeed such a reliable scheme that fulfils the requirements stated above is the central topic of this paper.

Before designing this calculation scheme, we would like to emphasize the following aspects (see also the Appendix):

(i) It has been shown[43] that a HF factorization when applied to a two-orbital model is capable to describe both the MH gap and the defect states emerging from the lower Hubbard band due to the defects. Even more important, the typical

multiplet splitting of the transition-metal ions is obtained if the factorization is performed with respect to an optimal local basis set, i.e., with occupation numbers either close to 1 or to 0. That is, the local spin-orbital states should be either occupied or empty.

(ii) This requirement leads to complications in the vicinity of defects. In particular, charge defects lead to a rotation of the occupied local states (see Sec. III) due to the Coulomb potential of a charged defect.

(iii) In principle, a local rotation can be specified that removes the off-diagonal terms and defines a new optimal local basis, i.e., orbitals having again integer occupancies (close to 1 or 0). This simple scheme, however, is not successful in presence of kinetic energy terms. Here, the optimal local or Wannier-type orbitals are influenced not only by local rotation terms, but by these nonlocal terms as well.

(iv) It is important to recognize that the full unrestricted HF scheme, i.e., including all relevant off-diagonal contributions from interactions, can be used to determine the MH-split bands in presence of defects. We will show here that this also holds true for the three-flavor case. In particular, we will show by comparison with ED that the approach provides a surprisingly good description not only of occupied states, but also of the unoccupied higher multiplet states.

(v) Moreover, the local rotated basis may serve as an intermediate basis and allows one to understand more easily the new features emerging due to the defects. For example, due to local rotation of t_{2g} orbitals, the flavor conservation in hopping processes that contribute to the kinetic energy is lifted in the rotated basis. That is, in the vicinity of defects, orbital flavors mix not only due to local orbital rotation (off-diagonal CF terms), but also due to the kinetic energy.

Except for a special attention to all relevant off-diagonal Fock terms, the unrestricted HF procedure applied here is a standard approach for tight-binding models of interacting electrons.[86–88] In general, one decouples each term describing a two-particle interaction and replaces it by all possible one-particle terms coupled to certain effective mean fields: density terms in the Hartree approximation (HA), supplemented by off-diagonal Fock terms in the HF approximation. Such expressions are augmented by double-counting correction terms, which are necessary to avoid double counting of the interaction energy. We will adopt just Hartree terms in only two cases: (i) when the interaction simulates a potential of the lattice and Fock terms would simply be out of scope (as for the JT terms), and (ii) when there is no one-particle term in the original Hamiltonian that can act as a source potential for the related off-diagonal mean fields (e.g., H_U with respect to spin degree of freedom). Note that the JT terms simulate the potential acting on pairs of neighboring V^{3+} ions due to lattice distortions and discriminating between the orbital flavors in the doublet $\{a,b\}$.

As a matter of fact, Fock terms become active only if their off-diagonal mean fields are finite. This can happen only if either a one-particle term in the original Hamiltonian (a source for the specific off-diagonal mean field) induces their finite value or we choose, as an initial state of the self-consistent procedure, a state that requires them to be finite. This second case is never realized in the studies we perform in this paper. Accordingly, we will adopt only Fock terms that couple either the same orbitals at neighboring sites (as in the kinetic energy) or couple different orbitals at the same site (as in the orbital-polarization interaction term $\propto D$). These latter Fock terms will turn out to be of fundamental importance to describe faithfully the physics of t_{2g} electrons in presence of defects. We remark that the HA is applied to the onsite interactions H_U in a way similar to that used to implement local Coulomb interactions within local density approximation (LDA) in the so-called LDA + U method.[89]

Given the above prescriptions, the derivation of the unrestricted HF equations is standard and we do not present it here *in extenso*; more details can be found, for instance, in Refs. 86 and 87. Following this procedure, one arrives at an effective one-electron HF Hamiltonian

$$\mathcal{H}_{\rm HF} = \sum_{i\alpha\sigma} \varepsilon_{i\alpha\sigma} n_{i\alpha\sigma} + \sum_{i\alpha\mu\sigma} \beta_{i\alpha\mu\sigma} c^\dagger_{i\alpha\sigma} c_{i\mu\sigma} + \sum_{\langle ij\rangle} \sum_{\alpha\mu\sigma} t^{\gamma}_{i\alpha j\mu;\sigma} c^\dagger_{i\alpha\sigma} c_{j\mu\sigma} \,. \tag{2.23}$$

This Hamiltonian can be diagonalized numerically, and the mean fields appearing in the parameters (see below) of the HF Hamiltonian (2.23) and the HF orbitals can be determined self-consistently within an iterative procedure. The orbital energies $\varepsilon_{i\alpha\sigma}$ are defined as follows:

$$\begin{aligned}\varepsilon_{i\alpha\sigma} = {}& \varepsilon^0_c \delta_{c\alpha} + U\langle n_{i\alpha\bar\sigma}\rangle + (U-2J_H)\sum_{\mu\neq\alpha}\langle n_{i\mu\bar\sigma}\rangle \\ & + (U-3J_H)\sum_{\mu\neq\alpha}\langle n_{i\mu\sigma}\rangle + \sum_{j(i)} V_{ij}\langle n_j\rangle + V_D \sum_{\mathbf{m}\in\mathcal{D}} \xi_{im} \\ & + \frac{1}{2} V_{ab}(\delta_{a\alpha} - \delta_{b\alpha}) \sum_{j(i)\in ab} \langle \tau^z_j\rangle \\ & - \frac{1}{2} V_c(\delta_{a\alpha} - \delta_{b\alpha}) \sum_{j(i)\in c} \langle \tau^z_j\rangle \,. \end{aligned} \tag{2.24}$$

We have introduced the orbital moments $\langle \tau^z_j\rangle$ for the nearest neighbors j of the considered site i in the same plane ab and along the c axis, respectively, labeled $j(i)$. The parameter $\xi_{im} = 1$ if the site i belongs to a cube which surrounds a particular defect labeled by m in Eq. (2.11), i.e., $i \in \mathcal{C}_m$, and $\xi_{im} = 0$ otherwise. The above equations may be further simplified by introducing total electron densities $\{n_i\}$ and magnetizations $\{m_i\}$ at site i and electron densities $\{n_{i\alpha}\}$ and magnetizations $\{m_{i\alpha}\}$ per orbital α at site i:

$$n_i \equiv \sum_{\alpha\sigma} \langle n_{i\alpha\sigma}\rangle, \tag{2.25}$$

$$m_i \equiv \sum_{\alpha} \langle n_{i\alpha\uparrow} - n_{i\alpha\downarrow}\rangle, \tag{2.26}$$

$$n_{i\alpha} \equiv \sum_{\sigma} \langle n_{i\alpha\sigma}\rangle, \tag{2.27}$$

$$m_{i\alpha} \equiv \langle n_{i\alpha\uparrow} - n_{i\alpha\downarrow}\rangle. \tag{2.28}$$

One finds

$$\begin{aligned}\varepsilon_{i\alpha\sigma} = {}& \varepsilon^0_c \delta_{c\alpha} + \left(U - \frac{5}{2}J_H\right) n_i - \frac{1}{2}(U-5J_H) n_{i\alpha} \\ & - \frac{1}{2}\sigma(U-J_H) m_{i\alpha} - \frac{1}{2}\sigma J_H m_i + \sum_{j(i)} V_{ij}\langle n_j\rangle + V_D \xi_i \end{aligned}$$

$$+\frac{1}{2}V_{ab}(\delta_{a\alpha}-\delta_{b\alpha})\sum_{j(i)\in ab}\langle\tau_j^z\rangle$$
$$-\frac{1}{2}V_c(\delta_{a\alpha}-\delta_{b\alpha})\sum_{j(i)\in c}\langle\tau_j^z\rangle. \quad (2.29)$$

Note that the onsite charge repulsive term $U(n_i-\frac{1}{2}n_{i\alpha})-\frac{5}{2}J_H(n_i-n_{i\alpha})$ does not contain self-interactions. The terms that depend on magnetic moments $\{m_{i\mu}\}$ are responsible for the magnetic order found in the realistic regime of parameters (see Secs. V and VI). In the weak-coupling regime, where the system is metallic, these terms give magnetic instabilities driven by the Stoner parameter,[90] being in the present three-orbital model $I_{\rm HF}=U+2J_H$.

Near the defect at site m, one finds the local off-diagonal elements of the HF Hamiltonian $\beta_{i\alpha\mu\sigma}$ at site $i\in\mathcal{C}_m$ given by the orbital-polarization term (2.12) and by the Fock terms of the Coulomb interaction

$$\beta_{i\alpha\mu\sigma}=\sum_{\mathbf{m}\in\mathcal{D}}\xi_{im}\{D\lambda_{\alpha\mu}(\mathbf{r}_i-\mathbf{R}_m)-(U-3J_H)\langle c^\dagger_{i\mu\sigma}c_{i\alpha\sigma}\rangle\}, \quad (2.30)$$

where the parameters $\{\xi_{im}\}$ are defined as in Eq. (2.24). As we show in Secs. III and IV, the second term in Eq. (2.30) is crucial for $D\neq 0$ as it renormalizes the orbital mixing term $\propto D$ and makes it possible to find the orbitals that optimize the energy of the system. The hopping parameters $t_{i\alpha j\mu\sigma}$ are renormalized by the Fock term that stems from the intersite Coulomb interaction (2.18),

$$t_{i\alpha j\mu\sigma}=t^\gamma_{a\mu}-V_1\langle c^\dagger_{j\mu\sigma}c_{i\alpha\sigma}\rangle, \quad (2.31)$$

and this renormalization is, for instance, responsible for the different bandwidths of the minority and the majority bands in transition metals.[87] According to the nearest-neighbor nature of the "source" term (the kinetic energy), also the related Fock terms stem from the nearest-neighbor Coulomb interaction matrix element V_1. As a matter of fact, as discussed above, all other Fock terms will simply vanish.

C. Undoped Mott-Hubbard insulator

We begin with discussing the reference electronic structure of the two phases with broken symmetry in spin and orbital space relevant to YVO_3: the CG phase and the GC phase. The spin and orbital orders in these phases are shown schematically in Figs. 1(b) and 1(c), respectively. Unrestricted HF calculations have been performed for an $8\times 8\times 8$ supercell with PBC; larger systems have also been considered. In the case of an undoped system, a smaller supercell such as $6\times 6\times 6$ or even $4\times 4\times 4$ would suffice as the HF convergence is indeed very fast and the final results for charge, spin, and orbital density distributions as well as for the total and orbital resolved density of states (DOS) do not depend on system size, in both symmetry-broken phases, for sufficiently large N ($N\geqslant 4$). Within our numerical studies, we have used several parameters which are considered realistic for YVO_3, but here we present only the representative results obtained for two parameter sets given in Table I.

In the relevant regime of parameters for the RVO_3 perovskites, the electrons in undoped YVO_3 are localized as in a Mott insulator. We consider here the same set of parameters as used previously in Refs. 25 and 43: $t=0.2$ eV, $\varepsilon_c^0=0.1$ eV, $U=4$ eV, and $J_H=0.6$ eV. The value of $t=0.2$ eV has been estimated using the charge-transfer model. For Hund's exchange J_H, we have adopted a value that is somewhat screened with respect to its atomic value $J_H^{\rm atom}=0.64$ eV.[25] Finally, the value of U has been selected in order to obtain a value for the superexchange parameter $J=4t^2/U=40$ meV, which is consistent with the results obtained in neutron scattering experiments for spin excitations.[78] As regards the JT parameters V_{ab} and V_c, we have chosen values that are in the expected range for $LaVO_3$.

TABLE I. Standard parameter sets used in the numerical calculations; all parameters are given in eV. Defect potential $V_{\rm D}$ (2.11) contributes only in doped systems.

Set	t	ε_c^0	U	J_H	V_{ab}	V_c	$V_{\rm D}$
A	0.0	0.1	4.0	0.6	0.03	0.05	1.0
B	0.2	0.1	4.0	0.6	0.03	0.05	1.0

The value of the CF potential $\varepsilon_c^0=0.1$ eV guarantees that, in absence of the orbital-polarization interaction D, the c orbital is occupied at each V^{3+} ion. In this parameter range, and as long as any defect is absent, one may simplify the calculation of the electronic structure in the HF approximation as the spin of the c electron determines the magnetic moment at each vanadium ion, which is in the high-spin (HS) state ($S=1$) due to finite Hund's exchange. In this respect, the HF calculations reduce to those performed within the simplified two-flavor model.[43] Depending on the starting initial conditions, one finds two locally stable configurations, the CG and the GC phases shown schematically in Figs. 1(a) and 1(b), with a uniformly distributed charge of two electrons at each vanadium ion.

The current self-consistent unrestricted HF calculations, performed in the undoped regime, give the electronic structures of the CG and the GC phases,[91] shown in Figs. 2 and 3. For the present parameters, t_{2g} electrons are fairly well localized (as $t\ll U$) and a broken-symmetry ground state is found. In such a case, the HF approach is rather successful and provides not only a good description of the occupied states, but also a quite satisfactory description of the excited ones. In fact, in the present case also the structure of the upper Hubbard band (UHB) is quite well reproduced. To demonstrate this, let us consider first the CG phase. At a representative atom in position (0,0,0) [see Fig. 1(b)], one finds the DOS with well-separated occupied states in the lower Hubbard band (LHB) and with empty states in the UHB, which consists of three peaks. The almost-classical ground state corresponds to an occupied wave function $|c\downarrow b\downarrow\rangle$. While the c electron is perfectly localized ($n_c\simeq 0.993$), the occupancy of the b orbital is somewhat lower than one, $n_b\simeq 0.977$. This is due to weak fluctuations of the orbital flavor between nearest-neighbor sites along the c axis, where all spins are aligned (C-AF) and orbitals alternate (G-AO). Consequently, the $|a\downarrow\rangle$ state has finite low-electron density ($n_a\simeq 0.016$).

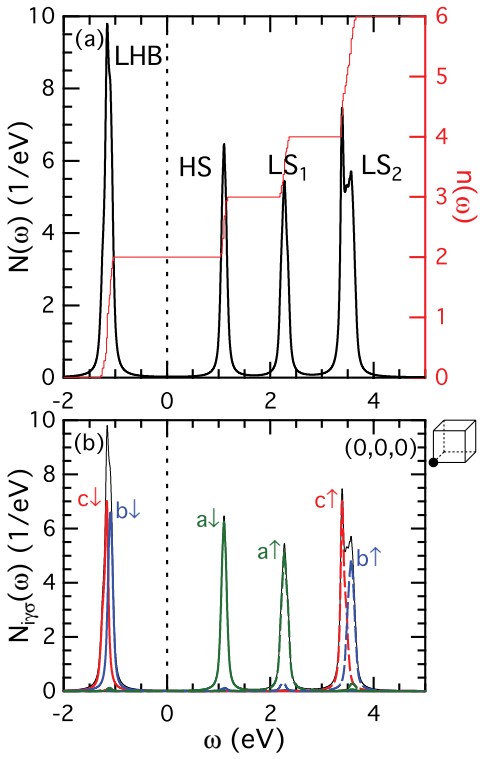

FIG. 2. (Color online) Densities of states for the Mott insulator in the CG phase calculated for an $8 \times 8 \times 8$ periodic cluster: (a) total DOS $N(\omega)$ (left scale) and the total electron filling $n(\omega)$ (right scale); (b) local spin-orbital DOSs $N_{i\alpha\sigma}(\omega)$ at the atom at site $i = (0,0,0)$, orbital α, and spin σ. The spectra reflect the spin-orbital order at (0,0,0) and $\downarrow$-spin ($\uparrow$-spin) states are drawn by solid (dashed) lines, respectively. Vertical dashed line indicates the Fermi energy at $\omega = 0$; parameters as in set B in Table I.

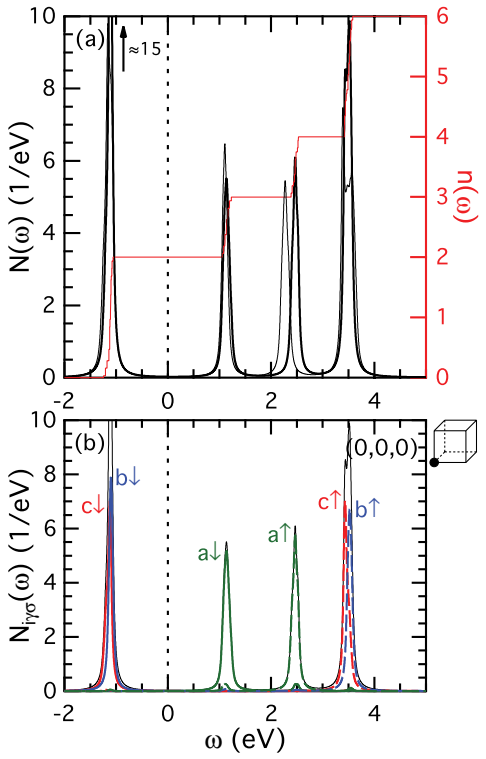

FIG. 3. (Color online) Densities of states as obtained for the Mott insulator in the GC phase for an $8 \times 8 \times 8$ system: (a) total DOS $N(\omega)$ (left scale, heavy line), the same for the CG phase (thin line) shown for comparison, and the total electron filling $n(\omega)$ (right scale); (b) local spin-orbital DOSs $N_{i\alpha\sigma}(\omega)$ at site (0,0,0), orbital α, and spin σ. Here, $\downarrow$-spin ($\uparrow$-spin) states are shown by solid (dashed) lines, respectively. Fermi energy and parameters as in Fig. 2.

The unoccupied part of electronic structure, the UHB, consists of three distinct maxima [see Fig. 2(a)]. The lowest one corresponds to the HS excitation and the system is a Mott insulator with a large MH gap: $\Delta_{\rm MH} \simeq 2.20$ eV. This value is obtained as the difference between the energies measured at the center of gravity (the first moment) of the peaks corresponding to the highest occupied and the lowest unoccupied HF orbitals: $|b\downarrow\rangle$ and $|a\downarrow\rangle$, respectively [see Fig. 2(b)]. Note that the value of the MH gap is given here by the energy of the HS charge excitation $d_i^2 d_j^2 \rightleftharpoons d_i^3 d_j^1$ to the $S = \frac{3}{2}$ spin state,

$$E_{\rm HS} = U - 3J_H\,, \tag{2.32}$$

with a $a^1 b^1 c^1$ configuration of $\downarrow$-spin electrons in the fully localized (atomic) limit.[17]

The UHB contains also low-spin (LS) excited states. As pointed out before,[43] their excitation energies obtained in the HF approximation (at $\varepsilon_c = 0$),

$$E_{\rm LS1} \simeq U - J_H, \tag{2.33}$$

$$E_{\rm LS2} \simeq U + J_H \tag{2.34}$$

are systematically lower by J_H than the exact ones and the upper state is doubly degenerate instead of the lower one, as the quantum-fluctuation driven processes (spin-flip and "pair-hopping" terms) are neglected.[92] For the considered ground state $|c\downarrow b\downarrow\rangle$, one finds first a LS ($S = \frac{1}{2}$) state with the $|a\uparrow\rangle$ state occupied [see Fig. 2(b)]. The energy of this excitation, measured from the energy of the highest occupied $|b\downarrow\rangle$ state, is $E_{\rm LS1} = 3.37$ eV, which is indeed very close to the value obtained from Eq. (2.33) in the atomic limit $(U - J_H) = 3.4$ eV. The two remaining LS states have energies $E^{(c)}_{\rm LS2} = 4.47$ eV and $E^{(b)}_{\rm LS2} = 4.64$ eV, corresponding to double occupancies in the c and b orbitals, respectively. These states have been labeled with the added electron to the ground state [$|c\uparrow\rangle$ and $|b\uparrow\rangle$ in Fig. 2(b)]. The above energies are again very close to the atomic limit values $\varepsilon_c + (U + J_H) = 4.5$ eV and $(U + J_H) = 4.6$ eV, respectively.

The maxima in the total DOS $N(\omega)$ are well separated from each other. This can be clearly seen in the total electron filling up to energy ω,

$$n(\omega) = \int_{-\infty}^{\omega} d\omega' N(\omega'), \tag{2.35}$$

which is almost constant in-between the maxima corresponding to different states [see Fig. 2(a)]. In particular, no states can be found within the MH gap.

The overall picture obtained for the GC phase is very similar, again with the LHB accompanied by three peaks in the UHB (see Fig. 3). In this case, the G-AF ground

state makes the electrons even more localized and one finds (down-spin) electron densities $n_c \simeq 0.993$, $n_b \simeq 0.989$, and $n_a \simeq 0$ at the representative (0,0,0) atom [see Fig. 1(c)]. The system is a good MH insulator with total electron filling $n(0) = 2$. A better electron localization than in the CG phase may also be concluded from a somewhat increased value of the MH gap, $\Delta_{\rm MH} \simeq 2.24$ eV. The low-spin excitations are found now at energies $E_{\rm LS1} = 3.57$ eV, $E^{(c)}_{\rm LS2} = 4.53$ eV, and $E^{(b)}_{\rm LS2} = 4.62$ eV. The largest difference with respect to the CG phase of 0.2 eV is found for the LS1 excitation energy $E_{\rm LS1}$ [see Fig. 3(b)]. We suggest that this increased excitation energy originates from a highly localized $(a\uparrow)$ component within the ab plane (in the GC phase) as the very same orbital is stronger localized here at the neighboring sites along the a and b directions than in the CG phase. We also note the increased height of the peaks, which indicates again stronger localization.

In summary, we have shown by the HF analysis of both CG and GC phases that the DOS consists of the LHB and the UHB, and that the latter has a well-defined internal structure of excited states. The MH gaps are very similar in both magnetic structures for the chosen set of parameters. In the next sections, we analyze the change of local electronic state near charged defects introduced by doping and show how such defects change the above idealized electronic structure.

III. OPTIMIZED ATOMIC ORBITALS

To develop systematic understanding of the evolution of the electronic structure under increasing doping, it is helpful to analyze first the atomic problem for a representative atom near a Ca defect embedded in the CG phase of YVO_3. Thus, we consider the atomic limit, i.e., no hopping ($t = 0$), as in the parameter set A of Table I. The HF mean-field terms act on the electronic states of such an embedded atom with the ground state $|c\downarrow b\downarrow\rangle$ [see Fig. 4(a)]. This problem is solved self-consistently in the HF approximation described in the previous section and the solution is systematically compared to the ED results obtained for the very same external mean fields.

Although the electronic configuration d^2 at an undoped V^{3+} ion in the vicinity of the defect does not change with respect to

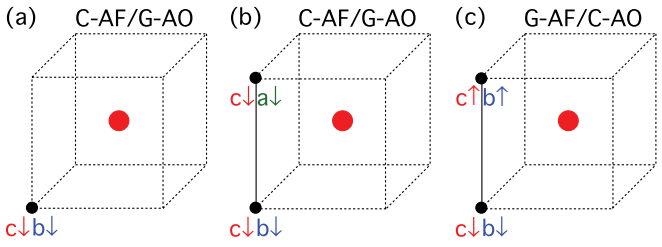

FIG. 4. (Color online) Reference electronic configurations considered in the reference ground state at $D = 0$ in Secs. III and IV for (a) a single atom (dot) in the CG phase; (b) a bond (solid line connecting two dots) along the c axis in the CG phase; (c) a bond (solid line connecting two dots) along the c axis in the GC phase. In each case, the state $|c\downarrow b\downarrow\rangle$ is selected as the initial ground state at the (0,0,0) atom. The relative position of the defect state in the center of each cube is marked by a filled (red) sphere.

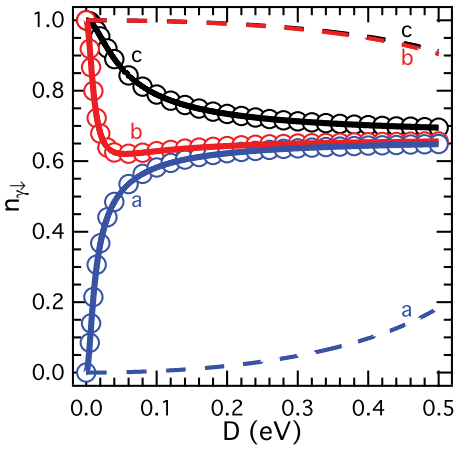

FIG. 5. (Color online) Electron densities $n_{\gamma\downarrow}$ in the pristine orbitals $\gamma \in \{a,b,c\}$ for an atom embedded in the CG phase [see Fig. 4(a)] as functions of increasing orbital polarization D. Solid lines from HF, dashed lines from HA, and hollow circles from ED. Parameters as in set A of Table I.

the Mott insulator described in Sec. II C, the occupied orbitals are now modified due to the electron polarization term (2.12). Here, we focus on the description of a single atom and compare the HF results with those of the ED with the aim at validating the scheme that will be used in Secs. V and VI for the bulk. The results are mainly presented for varying polarization parameter D, responsible for the adjustment of the orbitals to the field which acts on them.

The set of t_{2g} orbitals $\{a,b,c\}$ [Eq. (2.9)], also called *pristine* orbitals hereafter, is selected as orthogonal basis in the undoped YVO_3 by lattice distortions, which lower the c orbitals by a finite CF energy ε^0_c. *A priori*, t_{2g} orbitals are expected to adjust to the orbital-polarization field D in the vicinity of a defect and a new set of orthogonal orbitals will become the optimal basis for the embedded atom. We have determined this optimal basis using the self-consistent HF calculations described in the previous section and found that all three pristine t_{2g} orbitals $\{a,b,c\}$ are strongly modified; already for $D = 0.1$ eV, the occupied orbitals look quite different from $\{a,b,c\}$ ones (see the following). This gradual orbital rotation can be easily recognized by analyzing the electron densities $n_{\gamma\downarrow} \equiv \langle n_{\gamma\downarrow}\rangle$ and the off-diagonal elements of the density matrix $\langle c^\dagger_{\gamma\downarrow} c_{\xi\downarrow}\rangle$ shown in Figs. 5 and 6, respectively, for the CG phase.

The electron densities are $n_{c\downarrow} = n_{b\downarrow} = 1$ and $n_{a\downarrow} = 0$ for the reference state at $D = 0$. One finds that they change fast with increasing D for the orbitals a and b (Fig. 5), while the decrease in the electron density within the c orbital is slower. Therefore, in the weak polarization regime of $D < 0.02$ eV, the two-flavor model[43] is sufficient. On the contrary, for $D \simeq 0.1$ eV, all three orbitals contribute to the ground state with similar electron densities: the electron densities in the a and b orbitals are almost equal and $n_{c\downarrow} < 0.8$. Certainly, the two orbitals occupied in this case are quite different from the pristine c orbital and one of the doublet $\{a,b\}$ orbitals and the full orbital space have to be considered. This observation is further supported by the values of the off-diagonal matrix elements (Fig. 6), which become similar to

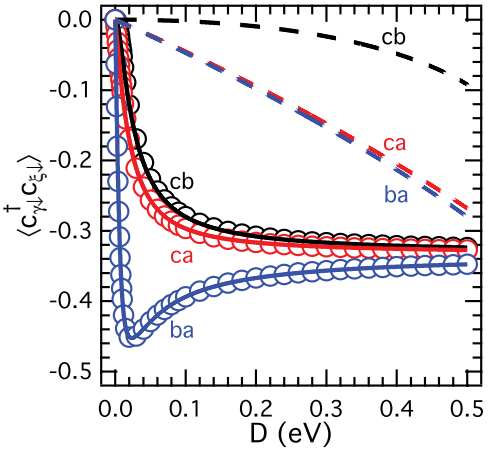

FIG. 6. (Color online) Off-diagonal elements $\langle c^\dagger_{\gamma\downarrow} c_{\xi\downarrow}\rangle$ $(\gamma \neq \xi)$ of the density matrix for spin-down pristine orbitals for an atom embedded in the CG phase [see Fig. 4(a)] as functions of increasing orbital polarization D. Solid lines from HF, dashed lines from HA, and hollow circles from ED. Parameters as in set A of Table I.

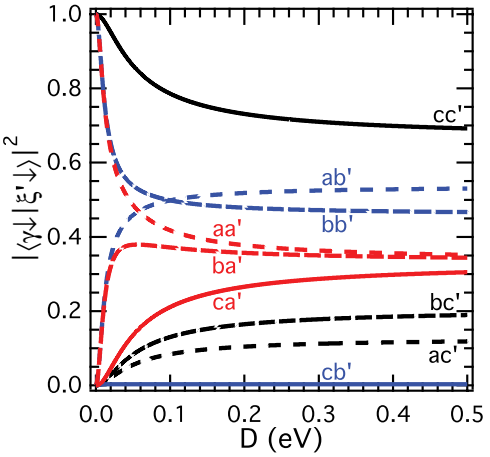

FIG. 7. (Color online) Fractions of pristine orbitals $\{|\gamma\rangle\}$ in the rotated orbitals $\{|\xi'\rangle\}$ for an atom embedded in the CG phase [see Fig. 4(a)] as functions of increasing orbital polarization D. Parameters as in set A of Table I.

each other for $D \simeq 0.1$ eV, while for $D < 0.02$ eV, the orbital mixing is large only between the a and b orbitals. For the largest value of $D = 0.5$ eV studied here, all three t_{2g} orbitals are almost equally occupied (Fig. 5) and the off-diagonal orbital elements are almost the same for each pair (Fig. 6).

It is very remarkable that the HF results presented in Figs. 5 and 6 agree exactly with the ED results. This shows that the quantum fluctuations, going beyond HF approximation, are irrelevant for the ground state in the present regime of parameters. In fact, the electron localization and the symmetry breaking in the spin and orbital space, which follow from the large value of U, suppress quantum fluctuations around the exact state with two occupied optimal orbitals. In contrast, the results obtained within the simpler HA (without Fock orbital terms) turn out to be completely unsatisfactory and this approximation gives an unrealistic description of the orbital states (see Figs. 5 and 6). Within HA, the orbitals b and c are almost unchanged and remain still the occupied orbitals even for relatively large values of $D > 0.1$ eV, where also their rotation (mixing) hardly occurs. This demonstrates that the Fock terms are essential in the present problem, as these off-diagonal terms are responsible for a gradual adjustment of the orbital subsystem to the orbital-polarization term (2.12), which drives the orbital mixing.

The gradual evolution of the two occupied rotated orbitals $\{|b'\rangle,|c'\rangle\}$ (and the unoccupied orbital $\{|a'\rangle\}$) relative to the original t_{2g} basis as function of the orbital-polarization field D is illustrated by the overlap functions $\langle\gamma\downarrow|\xi'\downarrow\rangle$ in Fig. 7. The initial state with occupied orbitals $\{|b\rangle,|c\rangle\}$ changes gradually with increasing D and the occupied orbitals $\{|b'\rangle,|c'\rangle\}$ are linear combinations of the pristine ones. One finds once more that, except for the region of rather small $D < 0.02$ eV, all three pristine orbitals contribute and the orbitals are strongly modified. The new states $|c'\rangle$ and $|a'\rangle$ arise as linear combinations of all three t_{2g} orbitals $\{a,b,c\}$. In contrast, the occupied orbital state $|b'\rangle$ has no component with $|c\rangle$ orbital character and is just a linear combination of $\{a,b\}$ orbitals. By considering solely this orbital state, one could therefore justify *a posteriori* the two-orbital model,[43] but we note that (i) the actual ground state involves the occupied $|c'\rangle$ orbital too, which has a significantly modified shape with respect to the original $|c\rangle$ state, and (ii) the presence of finite kinetic energy between such orbital states will induce a further redistribution of the pristine orbital character over the two occupied orbitals $\{|b'\rangle,|c'\rangle\}$, and will also modify the $|a'\rangle$ orbital contributing to excited states. The difference found here between the a and b orbital character in the occupied $|c'\rangle$ state follows from the mean fields that arise due to the JT interactions.

The local orbital basis gradually rotates and adjusts itself to the orbital polarization when D increases, as shown in Fig. 8. The Coulomb repulsion between the exceeding electron at the

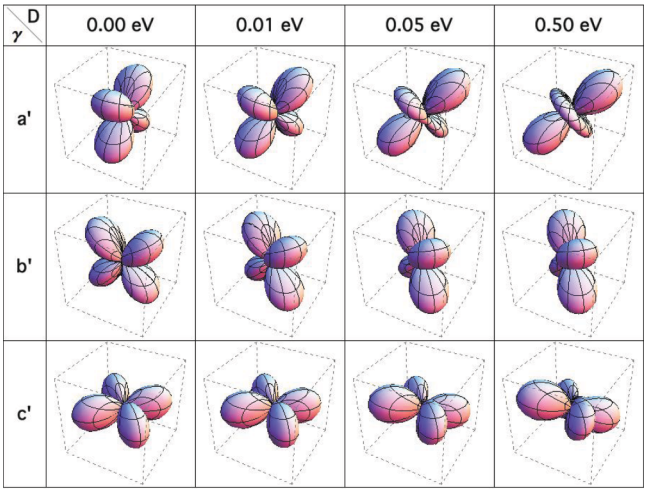

FIG. 8. (Color online) Optimal orbital basis for an embedded atom in the CG phase at position (0,0,0) [see Fig. 4(a)] for increasing orbital-polarization field D. The defect which is the source of the orbital-polarization term is located at position $(\frac{1}{2},\frac{1}{2},\frac{1}{2})$. The three rotated orbitals are labeled by $\gamma = a',b',c'$, with the orbitals b' and c' occupied in the ground state. At $D = 0$ eV (first column), $\{a',b',c'\}$ orbital coincides with $\{a,b,c\}$. Parameters as in set A of Table I.

Ca defect in the center of the V_8 cube [see Fig. 4(a)] and the V^{3+} ion adjusts the shape of the occupied orbitals $\{|b'\rangle,|c'\rangle\}$ in such a way that the electrons involved increase their distance from each other, and not too much of the JT and CF energy is lost. Therefore, the orbital shapes become all nonequivalent for $D > 0$ and evolve gradually into two geometrically similar occupied orbitals $\{b',c'\}$, with c' practically lying in the plane perpendicular to the direction along which the defect resides, and the empty cigarlike a' orbital, directed towards the defect site. This final configuration can be easily recognized at the largest studied value $D = 0.5$ eV. In the large-D regime, the rotated wave functions are

$$|a'\rangle = \frac{1}{\sqrt{3}}(|a\rangle + |b\rangle + |c\rangle), \tag{3.1}$$

$$|b'\rangle = \frac{1}{\sqrt{2}}(-|a\rangle + |b\rangle), \tag{3.2}$$

$$|c'\rangle = \frac{1}{\sqrt{6}}(-|a\rangle - |b\rangle + 2|c\rangle). \tag{3.3}$$

In a doped system, a hole will go into the topmost occupied orbital $|b'\rangle$, which is an odd linear combination of $|a\rangle$ and $|b\rangle$, and does not contain the third c flavor.

When D is finite and the CF term as well as the mean-field terms acting on the atom are neglected, the local problem given by the orbital polarization maps onto the hole-hopping problem on a triangle, with the energy spectrum $\{-D, -D, +2D\}$. Having two electrons at the V^{3+} ion, the two degenerate states with energy $-D$ are then occupied. The increasing similarity of the occupied states anticipated from this result is indeed observed when D increases in presence of other terms. In-between $D = 0$ and the largest value $D = 0.5$ eV studied here, one can distinguish two qualitatively different regimes: (i) for small $D \lesssim 0.02$ eV, only the orbitals $\{a,b\}$ mix, while the c orbital still does not change as it is stabilized by the CF energy $\varepsilon_c^0 = 0.1$ eV; (ii) when D becomes of the order of ε_c^0, the c orbital is destabilized and all three orbitals rotate further towards their final shapes. The case of $D \sim 0.05$ eV shown in Fig. 8 gives orbitals that are already close to those found at the largest studied value $D = 0.5$ eV. Note also that weak JT interactions counteract the orbital rotation, but the orbital polarization is the dominating term for the present set of parameters, and the basis rotation is practically completed already for $D \simeq 0.1$ eV (see Fig. 7).

Orbital polarization influences also the one-particle excitations of an atom close to a defect. Given the ground-state energy $E_0(d^n)$ of a Mott insulator in the d^n electronic configuration, these excitations in correlated insulators are calculated as follows: for exciting a hole, as in photoemission (PES) spectra,

$$E_m = E_m(d^{n-1}) - E_0(d^n); \tag{3.4}$$

and similarly for adding an electron, corresponding to inverse photoemission (IPES) spectra,[93]

$$E_m = E_m(d^{n+1}) - E_0(d^n). \tag{3.5}$$

We determined the excitation energies for an atom embedded in the CG phase in proximity of a defect using the unrestricted HF approximation and compared them with the corresponding ED results, as shown in Fig. 9. For the sake of convenience,

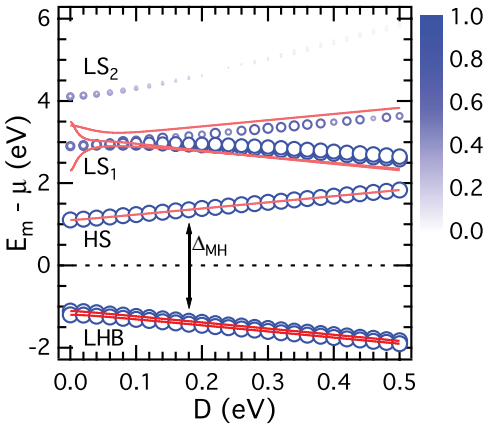

FIG. 9. (Color online) Excitation energies E_m for an atom embedded in the CG phase [see Fig. 4(a)] measured with respect to the chemical potential, as functions of increasing orbital polarization D. Solid lines from HF (heavy/light lines for occupied/unoccupied states) and hollow circles from ED (the color scale on the right indicates the spectral weight of each level, as well as the size of the symbols). The MH gap is found between the LHB and the HS state of the UHB; the labels of the LS excited states refer only to the regime $D \simeq 0$. The chemical potential μ is fixed at the center of the MH gap Δ_{MH}. Parameters as in set A of Table I.

the chemical potential μ, fixed as usual in the center of the MH gap, is subtracted in each case.

In the HF spectra, one finds two PES excitations that correspond to removing an electron either from b' or c' orbitals; the energy difference between them is small and comes from the CF splitting ε_c^0. These states form the occupied LHB. The apparent decrease in energy present in Fig. 9, $(\partial E_m/\partial D) \cong -1.5$ instead of the expected $(\partial E_m/\partial D) \cong -1$, follows from the subtraction of the chemical potential. The four excitations at positive energies correspond to the four possible d^3 excited states analyzed for the undoped case in Sec. II C: (i) the HS state has the lowest energy and the $|a\downarrow\rangle$ state is occupied; (ii)–(iv) in the three LS states with higher energies, a $\uparrow$-spin state is occupied in one of the three orbitals. Notably, these excitation energies depend rather strongly on the orbital polarization D. The energy of the HS state ($S^z = -\frac{3}{2}$) increases with increasing D when all three orbital flavors are occupied with the same spin, and $(\partial E_m/\partial D) \cong 2$ before chemical potential subtraction. As a matter of fact, such increase concerns also the LS2 excited state with $S^z = -\frac{1}{2}$ and $|c'\uparrow\rangle$ state occupied. On the contrary, the remaining two LS states of the UHB have either $(a'\uparrow)$ or $(b'\uparrow)$ occupations by the $\uparrow$ spin and their energies decrease. Note that the energies of the HS and of these latter LS excited states cross for a value of $D > 0.5$ eV, but we have estimated that so large values of D are unrealistic.

A comparison of the HF results with the exact results found using ED for an embedded atom close to a defect gives an excellent agreement for the LHB and even for the lowest HS excited state of the UHB. This may be expected as these three states have no quantum corrections. On the contrary, as already pointed out in Sec. II B, in the LS sector one finds that the excitation energies for $D = 0$ are lower by $\sim J_H$ than the exact values.[43] When D increases, the spectral weight

moves from the high-energy LS2 state with $E_m - \mu > 4$ eV to the lower-energy excitations with $E_m - \mu \sim 3$ eV. This is in contrast to the HF results, where the one-electron wave functions do not allow for any spectral weight transfer, and instead the excitation energies change and interpolate between the relevant energies in a continuous way. Already for $D \simeq 0.15$ eV, one finds that the spectral weight found in the ED has moved completely to the lower-energy regime characteristic of LS1 states, and when D increases further, there is one excitation with large spectral weight that follows roughly the two lower HF excitations of LS character, and the third one with increasing energy, similar to the one found in the HF (see above). Rather small energy difference between the ED energies and the HF ones found here demonstrates that the quantum effects are quenched in the orbital system when the orbital polarization D is sufficiently large. Even more importantly, a satisfactory agreement between the energies found in the HF approximation and the exact values in the LS sector shows that the HF states correctly adjust themselves to the underlying interactions and simulate the actual multielectron states in a very realistic way.

One may wonder again whether the HA would not give at least a satisfactory description of the excitations being close to the MH gap, as we have shown above that for all of them the quantum corrections to the HF energies are negligible. Instead, the HA fails also here in a rather spectacular way: one finds that the MH gap exhibits a qualitatively incorrect behavior and decreases with increasing orbital polarization D, and even the structure of the LHB, with two PES excitations of almost equal energies, is not correctly reproduced (see Fig. 10). Large systematic deviations are also found for the higher LS excited states. All these misleading features follow from the incorrect local basis rotation with increasing orbital polarization D, and thus from the incorrect evolution of the orbital electron densities shown in Fig. 5. It can be concluded that, at least in case of conflicting external fields (e.g., the CF, the JT interaction, and the orbital polarization), the HA is totally unsatisfactory.

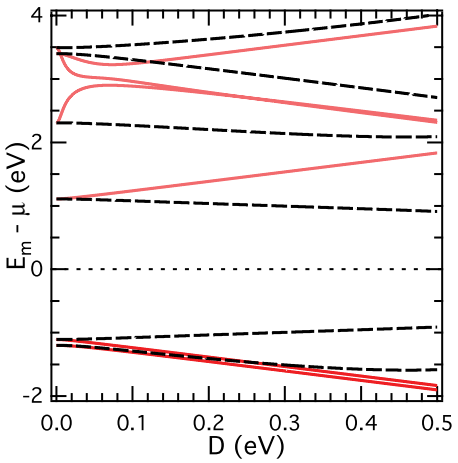

FIG. 10. (Color online) Excitation energies E_m for an atom embedded in the CG phase [see Fig. 4(a)] obtained in the HF (solid lines) and in the HA (dashed lines) for increasing orbital polarization D. The energies E_m are measured with respect to the chemical potential μ (dotted line). Parameters as in set A in Table I.

IV. A BOND NEAR THE DEFECT STATE

The electronic structure in the vicinity of defects depends also on the kinetic energy (2.5). While in the undoped bulk (Sec. II C), the kinetic energy is diagonal and couples two atomic t_{2g} states with the same orbital flavor at neighboring sites, this is no longer the case close to defects where the local orbital basis has to adjust to the actual fields acting on each atom (see Sec. III). Therefore, one expects that qualitative changes may arise with respect to the case of an embedded atom when electron hopping contributes. The analysis of an embedded bond presented in this section addresses this issue and serves to deepen and improve the understanding of the HF results presented for the bulk in the low-doping regime, analyzed in Secs. V and VI.

A. Electron densities induced by orbital polarization

We consider first a representative bond $\langle ij \rangle$ in the CG phase, shown in Fig. 4(b). The c orbitals are occupied at both sites of the bond (in the absence of defects, i.e., at $D = 0$) and the JT interactions (2.21) favor the b (a) orbital occupation at the lower (upper) site. This case is the most interesting one as the spin order is FM and the two electrons in the $\{a,b\}$ orbital doublet can delocalize along the bond. The kinetic energy is strongly suppressed by large local Coulomb interactions, but still one finds, within the ED, that orbital fluctuations along the bond contribute and modify the electron densities $n_{i\gamma\downarrow}$ for $\gamma = a,b$ at $D = 0$ (see Fig. 11). Such fluctuations are very important and support the FM coupling along the vertical bonds in the undoped material.[19] As we show below, the HF approximation may be still used although it is unable to treat orbitally entangled states,[24,28] as these fluctuations are quenched by external fields, including orbital polarization $D > 0$. In contrast, no fluctuations occur for the localized c electrons and their density is perfectly reproduced by the HF approximation.

As in the case of a single atom analyzed in Sec. III, an increasing orbital polarization D modifies the occupied orbitals and thus the electron densities (see Fig. 11). Full

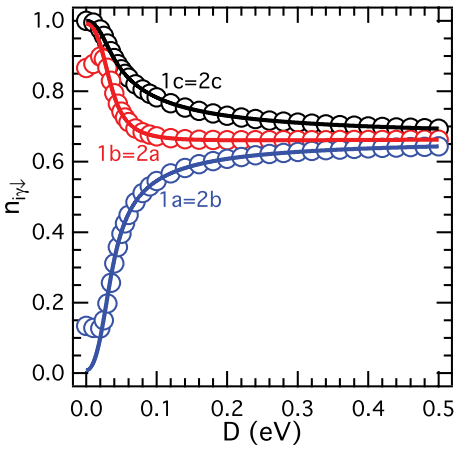

FIG. 11. (Color online) Occupations of pristine orbitals $n_{i\gamma\downarrow}$ at the embedded bond $\langle ij \rangle$ along the c axis in the CG phase [see Fig. 4(b)] as functions of increasing orbital polarization D. Solid lines from HF and hollow circles from ED. Parameters as in set B in Table I.

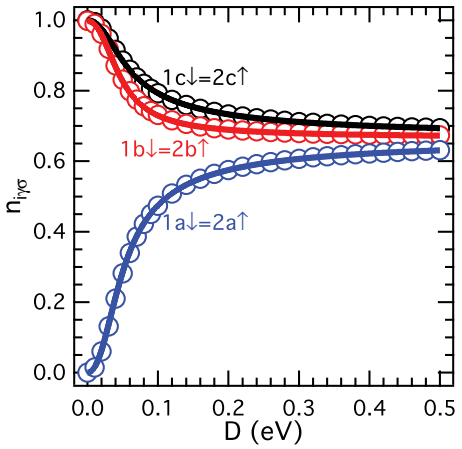

FIG. 12. (Color online) Occupations of pristine orbitals $n_{i\gamma\downarrow}$ at the embedded bond $\langle ij\rangle$ along the c axis in the GC phase [see Fig. 4(c)] as functions of increasing orbital polarization D. Solid lines from HF and hollow circles from ED. Parameters as in set B in Table I.

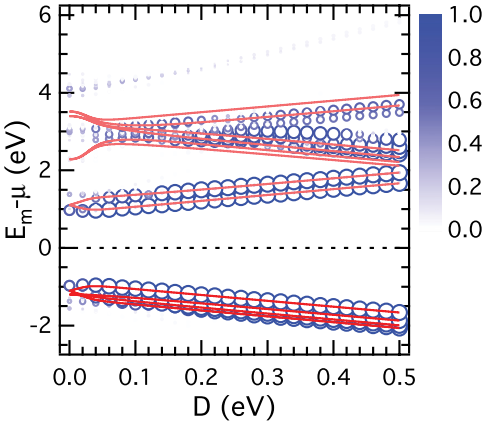

FIG. 13. (Color online) Excitation energies E_m for the embedded bond $\langle ij\rangle$ along the c axis within the CG phase [see Fig. 4(b)] as functions of increasing orbital polarization D. Solid lines from HF (heavy/light lines for occupied/unoccupied states) and hollow circles from ED (the intensity scale and marker size gives the spectral weight of each level). Parameters as in set B in Table I.

symmetry in the orbital occupancies is preserved, provided one interchanges the orbital flavors $\{a,b\} \leftrightarrow \{b,a\}$ between the sites $i = 1$ and $j = 2$. Similarly as in the embedded-atom case, the orbitals of the doublet active along the c axis mix easier, and this mixing competes with the JT effective interactions, which act on them at each site. The orbital polarization overrules the effective molecular fields, which act on the $\{a,b\}$ orbitals, already for $D = 0.03$ eV (see Fig. 11), and the trend in the ED results changes; in the regime of small D, the filling of the occupied $\{1b,2a\}$ orbitals $n_{1b\downarrow} = n_{2a\downarrow}$ first slightly increases with increasing D with respect to the one at $D = 0$, but next when D increases further it starts to decrease and the orbital entanglement is suppressed. In this latter regime, one again finds a perfect agreement between the HF and the ED results, which show once more that the HF method is very reliable for states with broken symmetry. Note that, as long as the orbital fluctuations dominate for very small values of $D < 0.02$ eV, the orbital electron densities almost do not change, being stabilized by the orbital entangled state that also counteracts the rotation of c orbitals in this regime. On the contrary, in the regime of large $D > 0.1$ eV, the electron densities are very similar to those found in Sec. III for an embedded atom (cf. Fig. 5).

It is of interest now to compare the evolution of electron densities with increasing D between the CG and the GC phases. The latter phase features much less quantum fluctuations, as the AF spin order is present here also along the c axis and finite electron hopping would generate LS states unfavored by Hund's exchange. Therefore, the hopping is suppressed also along vertical bonds in agreement with the double-exchange mechanism,[38] at least in the HF picture where quantum fluctuations are almost completely neglected. Therefore, even when the electron hopping is finite, the kinetic energy is totally suppressed in this symmetry-broken state at $D = 0$, and the electron densities are as in Eqs. (2.9) (see Fig. 12). When D increases, the orbital rotation towards the optimal orbital basis in the limit of large D takes place (see Fig. 8) and the orbitals are again locally adjusted by the orbital-polarization term. Notably, the electron densities for the initially filled $\{1b,2a\}$ and empty $\{1a,2b\}$ orbitals are here more distinct than in the CG phase as the kinetic energy, which helps to make the electronic distribution almost symmetric, is absent. Altogether, the excellent agreement found in this case between the HF and the ED results confirms the more classical character of the GC phase with respect to the CG one.

B. One-particle excitations

We determined also the excitation energies, defined in Eqs. (3.4) and (3.5), for the embedded bond. Overall, the results found for the CG phase (see Fig. 13) resemble those obtained for an embedded atom (see Fig. 9). A qualitatively new feature in the ED is the broadening of the Hubbard subbands, found for the LHB and for the individual excitations that belong to the UHB. This broadening comes from the action of the kinetic energy which mixes the occupied states at both sites of the bond $\langle ij\rangle$ leading to bonding and antibonding states that are modified by the JT effective interactions. As for the atom, U is the dominating energy scale and the MH gap increases linearly with D. There are four excitation energies that belong to the LHB and stem from two excitations at each ion of the considered bond. Having these splittings in the one-electron states, it is natural to expect that also the three-electron states will occur in certain energy intervals for each (HS or LS) excited state. The number of excited states in the HS states is two as there could be two states filled by three electrons, one at each site.

The analysis of the LS states is more subtle here than in the embedded atom case, as not only four LS2 states (two at each atom) split off with increasing D, but because also their spectral weight is transferred from the LS2 states to energies characteristic of the LS1 excitations. All in all, the qualitative picture found before for the embedded atom is confirmed here for the embedded bond, and again the LS1 excitations, which correspond to creating doubly occupied orbitals of b character or single occupations in the $a\uparrow$ orbital, stay roughly in the same distance from the LHB independently of the value of D,

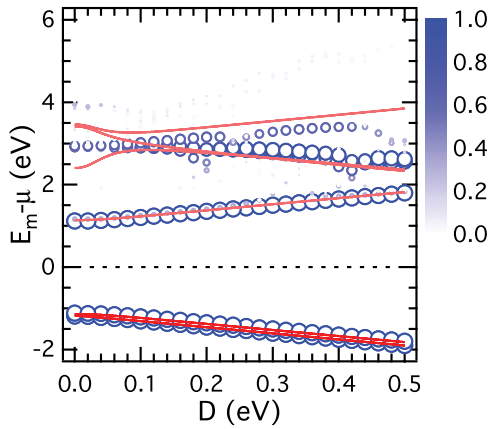

FIG. 14. (Color online) Excitation energies E_m for the embedded bond $\langle ij \rangle$ along the c axis within the GC phase [see Fig. 4(c)] as functions of increasing orbital polarization D. Solid lines from HF (heavy/light lines for occupied/unoccupied states) and hollow circles from ED (the intensity scale and marker size indicate the spectral weight of each level). Parameters as in set B in Table I.

while the LS excitations at higher energies are finally the ones that involve double occupancies in the c orbital. The distance between these states and the HS excitations is close to $3J_H$, the value deduced from the multiplet splitting.[17] We remark that the HF approximation gives excitation energies that reproduce quite well the values obtained within the ED. This holds in particular for the LHB and for the HS states of the UHB.

Given the more classical character of the GC phase, the LHB and the UHB are even more pronounced in this case (see Fig. 14). Here, the splittings arising from the finite kinetic energy and found in the CG phase are absent. Accordingly, the dependence of the one-hole (PES) and the one-electron (IPES) excitation energies is very similar to that found for a single embedded atom in this phase (not shown). The LHB consists of two excitations that correspond to adding a hole to one of the occupied orbitals: either the c orbital, at the lower energy because of the crystal field, or the orbital in the $\{a,b\}$ doublet locally favored by the JT interactions. These excitations have been found both in the ED and in the HF at exactly the same energies.

The situation for the electron excitations at high energy is again more subtle. Here, one finds in ED four LS excitations at energy U with respect to the ground state, and they split off with increasing orbital polarization D: the ones with a roughly constant energy distance from the LHB do correspond to the double occupancy of b orbital or single occupations in the $a\uparrow$ orbital, while the ones that follow from double occupancy of c orbital exhibit a similar energy increase with increasing D as the HS state. Already in the range of relatively small $D \sim 0.05$ eV, the spectral weight is transferred from the LS2 excitations to lower energies, and the excitation energy of $U + 2J_H$ is not observed in the ED results anymore.

Here again, the HF approximation reproduces all trends found in the ED results, but instead of the spectral weight transfer of the ED, one finds that the evolution of the HF wave functions simulates very well the ED findings at sufficiently large values of D. Systematic errors in the HF, due to the absence of quantum fluctuations, have been found only in the regime of small $D < 0.1$ eV, where the HF energies interpolate between the excitation energies $U - J_H$ and $U + J_H$ (lower by J_H than the corresponding ED values at $D = 0$) and the values expected from the ED at sufficiently large D. Altogether, the agreement between the HF and ED is better in the regime of large D, where the quantum effects in the orbital space are suppressed.

C. Localization by Coulomb interaction U

So far, the results have shown that the HF approximation provides a realistic description of the electron density distribution in the occupied orbitals as well as of the excitation energies. This latter feature is not guaranteed in the HF approach by itself, but follows here from the relatively large value of $U = 4$ eV, which drives the electron localization and suppresses quantum fluctuations [except for spin fluctuations, fluctuations related to the "pair-hopping" term in Eq. (2.16), and the orbital fluctuations along FM bonds]. Here, we show that the results obtained for the selected parameters are actually valid in a broad range of values for the Coulomb parameter U.

We fix Hund's exchange parameter $J_H = 0.6$ eV, which is responsible for the HS value ($S = 1$) at V^{3+} ions in the ground state of the undoped system YVO_3. Given this choice, we varied the parameter U in a quite broad range of values starting from $U = 2.0$ eV.[94] As we have shown in Fig. 13, a relatively small value of $D = 0.03$ eV suffices to suppress the orbital fluctuations along the considered c bond in the CG phase. In this regime of parameters, the excitation energies E_m given by the HF approximation are in reasonable agreement with the ED ones (see Fig. 15), and only the LS states have systematically lower energies than their ED counterparts, as discussed in Sec. III. As a matter of fact, this holds in the whole range of $U > 2.0$ eV, i.e., in the entire physical range of local interactions relevant for transition-metal oxides.[94]

The dependencies of the one-hole and the one-electron excitations on U are complemented by the electron densities projected onto the orbitals of t_{2g} symmetry shown in Fig. 16. The c orbitals are almost filled in the entire explored range

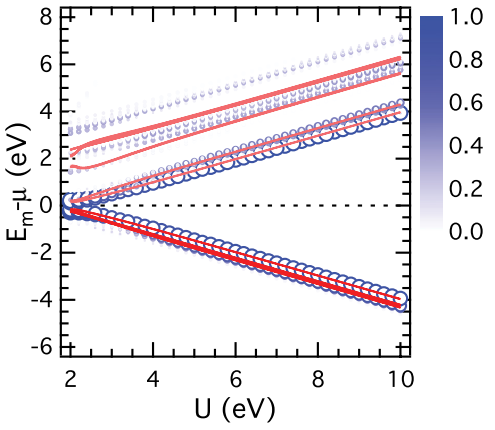

FIG. 15. (Color online) Energy levels in the embedded bond $\langle ij \rangle$ along the c axis within the CG phase [see Fig. 4(b)] as functions of increasing Coulomb interaction U for $D = 30$ meV. Solid lines from HF and hollow circles from ED (the intensity scale and marker size indicate the spectral weight of the level). Other parameters as in set B in Table I.

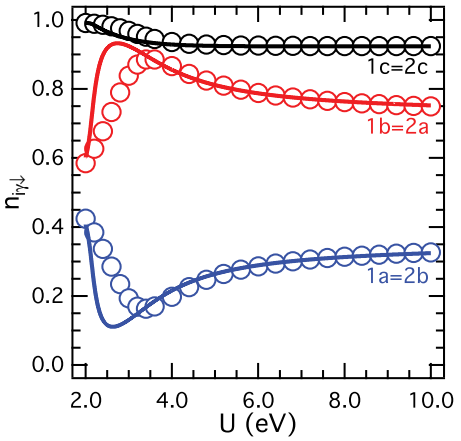

FIG. 16. (Color online) Occupations of spin-down pristine orbitals within the embedded bond $\langle ij\rangle$ along the c axis in the CG phase [see Fig. 4(b)] as functions of increasing Coulomb interaction U for $D = 30$ meV. Solid lines from HF and hollow circles from ED. Other parameters as in set B in Table I.

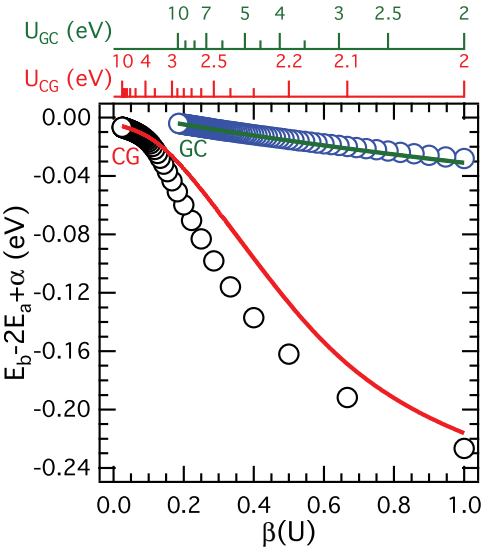

FIG. 17. (Color online) Hartree-Fock results (solid lines) for the superexchange contribution to the binding energy $\mathcal{E}_{\rm sex}(U)$ are compared to ED (circles) for an embedded bond $\langle ij\rangle$ along the c axis in the CG and the GC phases for $D = 30$ meV. For convenience, the U dependence is expressed by a nonlinear scale (top) and by the perturbative scaling functions $\beta_{CG}(U)$ (4.3) and $\beta_{GC}(U)$ (4.4), respectively. Other parameters as in set B in Table I.

of U. They are relatively robust with respect to orbital polarization for the present small value of $D = 30$ meV, but nevertheless the density n_{ic} gradually decreases from $n_{ic} = 1$ at $U = 2.0$ eV to $n_{ic} \simeq 0.92$ at large $U = 10$ eV. This evolution of the electron densities n_{ic} follows from the behavior of the orbital doublets $\{a,b\}$ at both sites.

First, in the regime of small U, electrons are not localized as the charge excitation energy is the same as the hopping parameter. The ED gives then the densities 0.58 (0.42) for the more (less) filled orbitals at the lowest considered value of $U = 2.0$ eV. The HF approach almost perfectly reproduces these densities. Increasing U suppresses the electron hopping along the bond, and the electron densities are gradually modified. The many-electron quantum state found in the ED is mainly determined by the fields acting on the orbital system: the JT effective fields from the neighboring atoms and the orbital-polarization term. In the regime of $U < 3.5$ eV, the change of the electron densities is markedly slower in the ED than in the HF approximation, as here quantum fluctuations contribute. Only for higher values of U, both calculations agree with each other showing once more that the HF approximation is reliable in the entire strongly correlated regime of large U due to the stabilization of symmetry breaking in spin-orbital space, which suppresses quantum fluctuations.

D. Ground state for the embedded bond

One may wonder how accurate the HF approximation is for the total energy of the considered bond. When the bond forms, one gains binding energy due to the kinetic energy. The binding energy can be computed as the energy difference between the energy of a bond and that of two single atoms:

$$\mathcal{E}(U) \equiv E_{\rm bond}(U) - 2E_{\rm atom}(U). \tag{4.1}$$

Thereby, one has to take into account the different numbers of neighbors in each case. An atom is surrounded by six neighbors, each of them providing mean fields acting on the orbitals. In contrast, each atom of the bond has just five external neighbors, while the interactions along the bond are rigorously (approximately) included in the ED (HF). This generates a correction term α to Eq. (4.1) included in Fig. 17, where we analyze the superexchange contribution to the binding energy $\mathcal{E}_{\rm ex}(U)$ defined as

$$\mathcal{E}_{\rm sex}(U) \equiv \mathcal{E}(U) - \mathcal{E}(\infty). \tag{4.2}$$

The binding energy $\mathcal{E}(U)$ [Eq. (4.1)] calculated in the ED can be compared with the strong-coupling approach of Ref. 25 to estimate the energy increments for the embedded bond and for the embedded atom in both magnetic phases: the CG and the GC phases. In the regime of large $U \gg t$, one finds asymptotic behaviors that suggest to use

$$\beta_{CG}(U) \equiv \frac{t}{U - 3J_H}, \tag{4.3}$$

$$\beta_{GC}(U) \equiv \frac{9t}{U - \frac{1}{3}J_H} \tag{4.4}$$

as scaling parameters. The value of $\beta_{CG}(U)$ [Eq. (4.3)] is obtained by considering HS excitations, while the value of $\beta_{GC}(U)$ [Eq. (4.4)] is derived as an average value over the LS excitations allowed in this case. These quantities have been used to plot the superexchange energy $\mathcal{E}_{\rm sex}(U)$ (4.2) for a single bond embedded in each magnetic phase considered here (see Fig. 17). We show the data for the same range of U values (2 eV $\leqslant U \leqslant$ 10 eV) adopted in Figs. 15 and 16, respectively, which correspond to $\beta(U) \leqslant 1.0$ in both phases, and $\beta_{CG}(U) > 0.024$ [$\beta_{GC}(U) > 0.183$] in the CG (GC) phase.

The analysis of the electron density distribution in Sec. IV C suggests that the local Coulomb interactions are sufficiently strong to localize the electrons if $U > 3.5$ eV (see Fig. 16), and one expects that the strong-coupling expansion in powers

of t/U should be valid. This is also confirmed by the present analysis of the binding energy $\mathcal{E}(U)$ [Eq. (4.1)]: the numerical results obtained from the ED and the HF method agree very well in this regime for the CG phase (see Fig. 17). Even more surprising is the fair agreement between the ED and the HF calculations found for smaller values of $U < 3.5$ eV (see Fig. 17). This result shows that the strong orbital quantum fluctuations in the CG phase along the c axis[19] are well accounted for within the unrestricted HF approach. In the GC phase, the agreement is even better and the dependence on $\beta_{GC}(U)$ is practically linear in the entire regime of considered values of U, i.e., for $U > 2.0$ eV. This confirms a quite strong electron localization in this phase, with the AF spin order preventing electronic transport and acting as a confining potential at each site of the bond.

V. DEFECTS IN THE DILUTE LIMIT

A. Orbital polarization and the electronic structure

The role of defects in transition-metal oxides is subtle due to strong electron correlations, which manifest themselves in the multiplet structure of the MH bands. As a result of the orbital degeneracy, strong orbital polarization and relevant relaxation processes occur in the vicinity of charged defects. Since a Ca defect replaces a Y-ion in YVO_3, each defect has eight vanadium neighbors that form a cube shown in Fig. 1; hence, the orbital degeneracy, which is controlled by the spin-orbital order in these compounds, is locally strongly affected by the defects.[43] The (occupied) orbitals in the neighborhood of the defect are polarized, i.e., rotated. This leads to a violation of the flavor conservation and, consequently, to a noticeable modification of the hopping matrix in the rotated t_{2g} basis. Moreover, for each Ca defect, a hole appears in its proximity, bound to it by the Coulomb potential of the charged defect itself. Since these holes can move, controlled by the double-exchange mechanism, they will affect the spin-orbital order further.[43] In addition, the chemical potential, due to the doped holes, will lie in a defect band inside the MH gap. Finally, also these defect states are subject to strong electronic correlations and display their own MH physics.

Our main aim here is to investigate whether the MH multiplet splitting can be reliably obtained within the unrestricted HF framework for the three-flavor t_{2g} case, i.e., in presence of defect potentials, various orbital-relaxation processes, kinetic energy of doped holes, and electron-electron interactions. Here, we consider the dilute limit of low-electron doping $x \leqslant 0.05$, where the defects can be treated as well separated from one another. For more clarity, we also limit ourselves to hole doping for only one orbital flavor and one spin. Therefore, to demonstrate this, we focus below on several rather transparent cases of increasing complexity:

(A) defect states in a multiband MH insulator in absence of orbital polarization and of Coulomb interaction among the electrons;

(B) role of orbital polarization;

(C) role of LR electron-electron interaction (Coulomb gap of defect states);

(D) orbital polarization and relaxation of Coulomb gap of defect states.

For the sake of clarity and simplicity, we will not consider here the effect of LR defect potentials and the self-consistent screening of LR interactions, which results from the doping induced by the impurities. As our focus is on the strong-correlation aspects and in order to get easy-to-interpret eigenstates and spectral distributions, we shall not discuss the effects of disorder here, i.e., the defects will always be well annealed and in the dilute limit.

B. Order-parameter landscape and defects

Unrestricted HF approach allows us to treat large inhomogeneous systems, i.e., with defects, interfaces, nanostructures, etc. We have seen earlier for a two-flavor model that the Mott-Hubbard gap and the multiplet structure are faithfully reproduced for the strongly correlated transition-metal oxide systems. A central requirement of the unrestricted HF to work is broken spin and orbital translational symmetry. Accordingly, vanadate perovskites, such as $Y_{1-x}Ca_xVO_3$, provide an ideal ground for this approach as spin and orbital orders in these compounds are present in a wide doping regime, actually up to the metal-insulator transition. Therefore, the unrestricted HF is the method of choice in our case. Nevertheless, it is not clear *a priori* how well the method works in the vicinity of defects in view of orbital polarization and hole motion. To explore this is our central goal.

Moreover, the HF provides a basis for subsequent many-body perturbation treatments. However, it should be noted that here such a perturbative treatment will not be performed with respect to an "uncorrelated" $U = 0$ state, but with respect to the HF ground state. This latter state already features the MH gap and the higher multiplet structure. In fact, it was already pointed out that the fundamental MH splitting, i.e., the energy difference of the LHB and the high-spin Hubbard band $\Delta_{\rm HS} = (U - 3J_H)$ is obtained exactly within HF. We shall see in the following that there are other gaps, e.g., between defect states, which suffer from the well-known overestimation of gap energies within HF theory. A subsequent many-body perturbation treatment of the screening of interactions is expected to cure such deficiencies of the HF approach.

In general, HF calculations require a self-consistent optimization of all expectation values that define the final HF Hamiltonian, the HF ground state, and the excitations. Complete information to construct the HF Hamiltonian is thus contained in the *order-parameter landscape*, which is defined by the full set of effective fields. It contains already the rotations of occupied (and unoccupied) orbitals due to defects and doping. As an example, we display the diagonal occupation numbers in the CG phase for the three-flavor calculation performed with PBC in Fig. 18. It shows maps of local magnetizations

$$m_\gamma(k,l,m) = n_{\gamma\uparrow}(k,l,m) - n_{\gamma\downarrow}(k,l,m) \qquad (5.1)$$

for an $8 \times 8 \times 8$ cube of V ions and, from left to right, for the orbital character $\gamma = c,b,a$ and $a+b$. Two planes are presented: the top row represents the front face of the cube at $l = 0$, while the bottom row shows the $l = 1$ plane.

The left panels reflect the C-type magnetic order of the electrons in c orbitals. The central panels show the same magnetic order for the b and a electrons. Here, in addition,

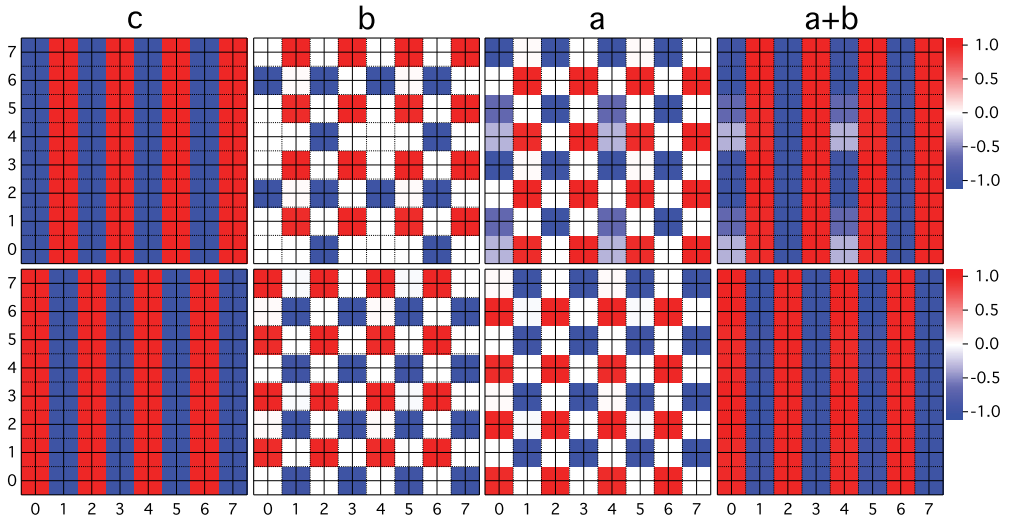

FIG. 18. (Color online) Map of the orbital magnetization densities $m_\gamma(k,l,m)$ [Eq. (5.1)] in the dilute well-annealed CG phase with $x = 0.015\,625 = \frac{1}{64}$, obtained for a $8 \times 8 \times 8$ cluster [from positive to negative $m_\gamma(k,l,m)$, see color scale on the far right]. The coordinates $k = 0, \ldots, 7$ are along the horizontal axis, and $m = 0, \ldots, 7$ along vertical axis, while the top row represents the $l = 0$ and the bottom row the $l = 1$ plane. Four panels (from left to right) for different orbital flavor: $\gamma = c$, $\gamma = b$, $\gamma = a$, and $\gamma = a + b$, respectively. Parameters: $V_{\rm ee} = 0$, $V_{\rm D} = 1$ eV, and $D = 0$, others as in set B in Table I.

one recognizes a checkerboard structure, which represents the G-type orbital order of the a and b electrons. In the right panel, magnetic densities of electrons in a- and b-type orbitals are summed up and reveal again the C-type magnetic structure. While the magnetization density has a perfect alternation between two sublattices in the $l = 1$ plane, four defects disturb it in the $l = 0$ layer (top row), as seen for b and a orbitals, and also for their sum.

The number of defects in the system corresponds in this case to hole doping $x = \frac{1}{64}$. Here, the arrangement of the defects is well annealed, i.e., LR defect repulsion has been considered and, therefore, the defects are regularly spaced. The defects are visible in the top panel of Fig. 18 and are located between the planes $l = 0$ and 1. The perpendicular feature in the $a + b$ panel reflects the motion of the doped holes along the c direction, but bound to the respective defects. From the b panel, one can also see that all four holes in the $l = 0$ plane have b-down character, as assumed. We next analyze the one-particle excitation spectra for such a cluster obtained in the HF approach.

C. Excited states in the three-flavor model

In the following, we shall investigate the HF excitation spectra for the four scenarios (A)–(D) introduced above. We will analyze only the CG phase as this phase is the relevant one for moderately doped $Y_{1-x}Ca_xVO_3$, and we first focus on the dilute doping case of $x = \frac{1}{64}$.

(A) We begin the discussion with the first scenario, where orbital-polarization effects and LR Coulomb interactions are not considered, i.e., $D = 0$ and $V_{\rm ee} = 0$. The strong defect potential $V_D = 1.0$ eV confines a single-doped hole per defect to the nearest-neighbor V sites of a defect, which form a cube. The corners of the V_8 cube are equivalent with respect to the defect potential yet not with respect to the spin and orbital orders. This implies that a $(b\downarrow)$ hole can delocalize only along a (vertical) bond along the c axis because of the AF order in the (horizontal) ab plane. The kinetic energy of the a and b electrons in the ab plane is quenched due to the double-exchange-type coupling to the spins of the c electrons.[43]

To explore this symmetry breaking and its consequences for the excitations, we investigate in Fig. 19 the total DOS $N(\omega)$ together with the local partial DOS $N_{i\gamma\sigma}(\omega)$ for the two sites (0,0,0) and (0,0,1) of the *active bond*, i.e., the bond doped with a hole, and for a site (1,1,0) on an undoped *spectator bond*. The chosen spectator bond corresponds to the same spin polarization as the active bond, thus in principle the hole could delocalize into its states too. However, this is not observed for the typical range of values of t (and other parameters). The total DOS in Fig. 19(a), obtained for the $8 \times 8 \times 8$ cluster, shows the same multiplet splitting as discussed for the atom in Sec. III. We recognize the LHB and the three multiplet subbands forming the UHB. The fundamental MH gap opens between the LHB and the HS subband of the UHB; the splitting of these bands is given by the gap

$$\Delta_{\rm HS} = E_{\rm HS} - E_{\rm LHB} = U - 3J_H, \tag{5.2}$$

and is reproduced exactly in the HF approach. In contrast, the actual MH gap

$$\Delta_{\rm MH} = U - 3J_H - W_{\rm eff} \tag{5.3}$$

is reduced by an effective bandwidth $W_{\rm eff}$. Due to the defects and their potentials, defect states are split off from the LHB. In other words, all single-particle states in the vicinity of the defect are shifted upwards by the defect potential V_D (for simplicity, we consider here only the case of a nearest-neighbor defect potential). These states lie now inside of the MH gap. The transitions from the occupied defect states D to the upper HS Hubbard subband define the in-gap absorption and the optical absorption gap which we denote $\Delta_{\rm opt}$. At the same time, the spectral weight moves out of the LHB, similar as in the doped Hubbard model.[95]

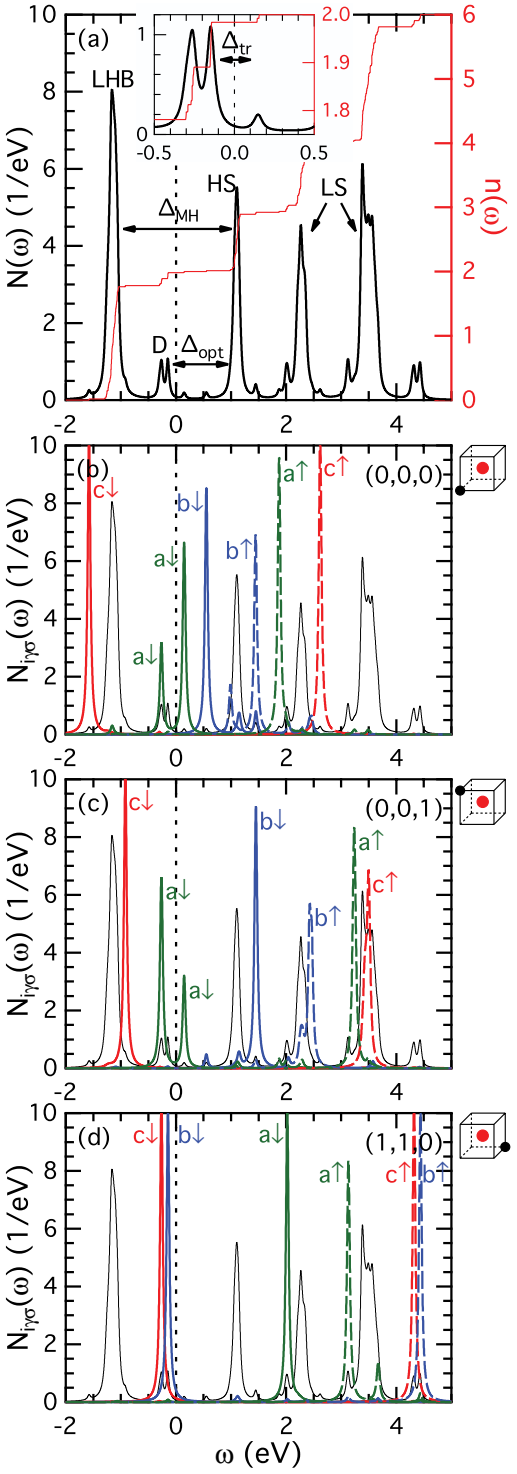

FIG. 19. (Color online) (a) Total DOS $N(\omega)$ (left scale) and average electron filling $n(\omega)$ (right scale) in the dilute well-annealed CG phase with defect concentration $x = \frac{1}{64}$, obtained using an $8 \times 8 \times 8$ cluster. The inset shows $N(\omega)$ near the Fermi energy $\omega = 0$. Panels (b)–(d) show individual DOSs $N_{i\alpha\sigma}(\omega)$ for orbital α and spin σ, together with the total DOS $N(\omega)$ (thin lines). The atom coordinate (0,0,0), (0,0,1), or (1,1,0) is indicated in each case and on the cube represented near each panel on the right. Parameters as in set B in Table I, and $D = 0$, $V_{ee} = 0$.

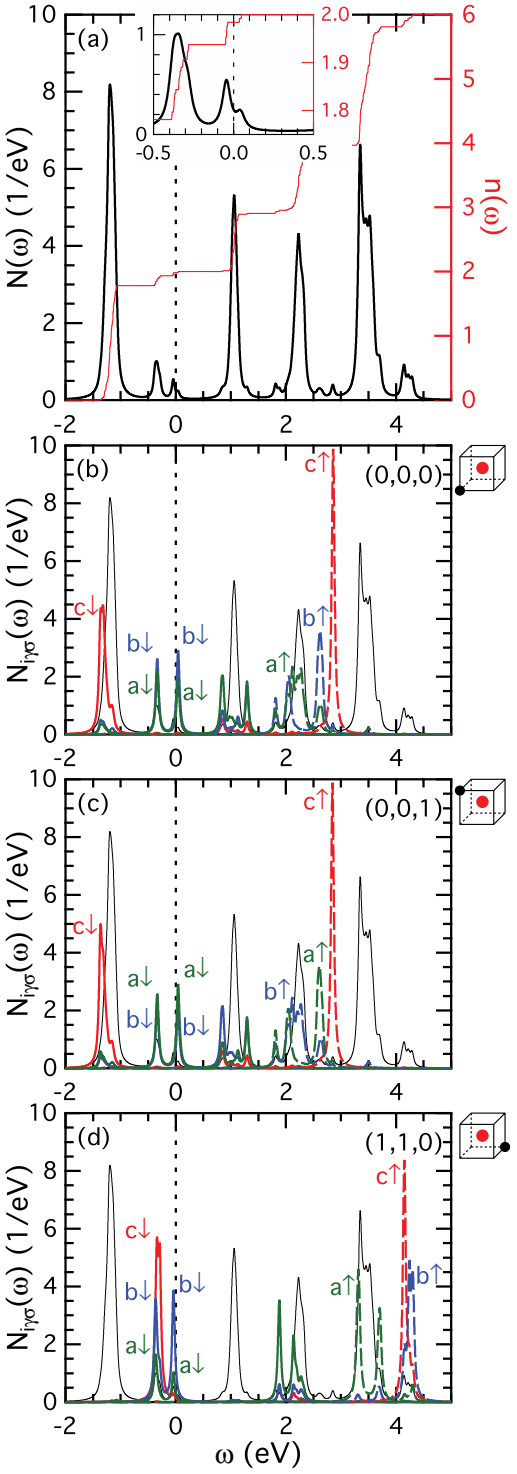

FIG. 20. (Color online) (a) Total DOS $N(\omega)$ (left scale) and average electron filling $n(\omega)$ (right scale) in the dilute well-annealed CG phase with defect concentration $x = \frac{1}{64}$, obtained using an $8 \times 8 \times 8$ cluster. The inset shows $N(\omega)$ near the Fermi energy $\omega = 0$. Panels (b)–(d) show individual DOSs $N_{i\alpha\sigma}(\omega)$ for orbital α and spin σ, together with the total DOS $N(\omega)$ (thin lines). The atom coordinate (0,0,0), (0,0,1), or (1,1,0) is indicated in each case and on the cube represented near each panel on the right. Parameters as in set B in Table I, and $D = 0.05$ eV, $V_{ee} = 0$.

The defect states would be completely filled, if there were not one doped hole per defect. This fixes the chemical potential μ inside the defect band. It is useful to consider the integrated (averaged) electron density $n(\omega)$ per site [Eq. (2.35)] displayed in Fig. 19(a) (see right scale). The chemical potential μ is then determined from the average of μ^- and μ^+, which are obtained from the relation

$$n(\mu^{\pm}) = n_0 - x \pm \epsilon \tag{5.4}$$

in the limit $\epsilon \to 0$, where $n_0 = 2$ is the average number of electrons per site in the undoped three-flavor model and x is the defect (hole) concentration. As can be seen from the inset in Fig. 19(a), the chemical potential falls into a small gap at the upper edge of the defect band D. In the following, we denote this gap as the *transport gap* $\Delta_{\rm tr}$ as it would be a relevant measure for the conduction in the defect band.

Deeper insight into the nature of the defect states and the transport gap is obtained by considering the local partial DOS $N_{i\gamma\sigma}(\omega)$, shown in Figs. 19(b)–19(d) for sites (0,0,0) and (0,0,1), which form the *active bond*, and at the (1,1,0) V ion, a *spectator site* with two electrons. The defect, indicated by a red dot, lies in the center of the cube at $(\frac{1}{2},\frac{1}{2},\frac{1}{2})$. The two electrons at the spectator site (1,1,0) occupy the $(c\downarrow)$ and $(b\downarrow)$ local orbitals as can be seen from Fig. 19(d). They lie below the chemical potential μ indicated by the perpendicular dashed line.

The doped hole has $(b\downarrow)$ character and is localized on the active bond displayed in Figs. 19(b) and 19(c). On both sites, the $(c\downarrow)$ orbitals are occupied, while the remaining $(a\downarrow)$ electron can delocalize on the vertical bond, i.e., parallel to the c axis, consistently with the FM correlations in the C-AF phase. This delocalization leads to a splitting into bonding and antibonding states on the active bond

$$\Delta_{\rm BA} \sim 2\sqrt{V_{\rm JT}^2 + t^2}, \tag{5.5}$$

where the bonding-antibonding gap $\Delta_{\rm BA}$ is determined by the resonance integral t and the JT interaction $V_{\rm JT} \approx V_{ab} - \frac{1}{4}V_c$ in the case of the G-AO order. In Figs. 19(b) and 19(c), $\Delta_{\rm BA} \approx 0.4$ eV is essentially determined by the hopping-matrix element $t = 0.2$ eV, while $V_{\rm JT} \approx 0.02$ eV. That the $|a\downarrow\rangle$ occupation is asymmetric along the active bond is a result of the JT interactions and the underlying G-type orbital order.

The origin of the "transport gap" $\Delta_{\rm tr}$ is evident in this case and we identify it here with the gap between the topmost occupied orbital on a spectator bond, i.e., $|b\downarrow\rangle$ orbital at site (1,1,0) and the unoccupied antibonding state on the active bond. This energy is

$$\Delta_{\rm tr} \sim \sqrt{V_{\rm JT}^2 + t^2} + V_{\rm JT}, \tag{5.6}$$

and for the present parameters one finds in Fig. 19 that $\Delta_{\rm tr} \approx 0.22$ eV, and is essentially determined by the kinetic energy. It is important to realize that within the HF scheme, occupied (unoccupied) orbitals correspond to electron removal (addition) energies. These processes need not refer necessarily to the same defect, but can occur at different defects. Thus, $\Delta_{\rm tr}$ is the energy gap for the hopping processes between different defects within the defect band.

The energies of the occupied $(c\downarrow)$ orbitals differ strongly at different ions [see Figs. 19(b)–19(d)]. This is a consequence of the different local occupation numbers, which enter the HF energies. Obviously, this also affects the energies of the unoccupied orbitals. The defect states have their own MH gap as can be seen, for example, in Fig. 19(d). Inserting an $(a\downarrow)$ electron on site (1,1,0), in addition to the already present $(c\downarrow)$ and $(b\downarrow)$ electrons, leads to the HS defect state $|c\downarrow b\downarrow a\downarrow\rangle$ at $\omega \sim 2.0$ eV. Finally, at higher energies, one recognizes the LS defect multiplet states $|c\downarrow b\downarrow\gamma\uparrow\rangle$, with $\gamma = a,b,c$, respectively.

(B) The effect of the Coulomb potential of the defect is to rotate the occupied orbitals in the vicinity of the defect such that their energy is minimized. This polarization effect, described by $H_{\rm pol}$ and controlled by the parameter D, was not considered in the first scenario. The second scenario represents a calculation within the same parameter set of the first scenario, with the exception for finite $D = 0.05$ eV. The total DOS $N(\omega)$ shows a clear change of the DOS of the defect states in the vicinity of μ, which is amplified in the inset of Fig. 20(a). While there was a pronounced transport gap in the absence of orbital polarization, here this gap has almost disappeared (or is of marginal size).

The main effects of orbital polarization can be revealed by inspecting the local partial DOS $N_{i\gamma\sigma}(\omega)$. As we observe in Figs. 20(b) and 20(c), which reflect the changes on the sites of the active bond, the $(c'\downarrow)$ orbital has now some admixtures of $(a\downarrow)$ and $(b\downarrow)$ flavors. More importantly, Figs. 20(b) and 20(c) show that the bonding and antibonding states are defined by linear combinations of $|a\downarrow\rangle$ and $|b\downarrow\rangle$ states, and have no longer pure $(a\downarrow)$ character, as it was the case in Figs. 19(b) and 19(c). This mixing is a consequence of the flavor nonconservation in the rotated t_{2g} basis and of the resulting off-diagonal terms in the kinetic energy.

The most important feature in this second (B) scenario is the formation of a bonding-antibonding splitting on the *spectator bond*, as can be seen in Fig. 20(d). At first glance, this may look puzzling as both states are occupied, so there is no obvious net energy gain that may drive such a splitting. Inspection of energies and occupation numbers shows that the level splitting is due to a combined mechanism: the rotation of the c orbital is favored when its energy coincides with the level of the bonding orbital. Thus, we observe here an *orbital rotation induced by bonding-antibonding splitting* on the spectator bonds.

Interestingly, the antibonding band on the spectator bond is pinned to (but remains below) the chemical potential, whereas the antibonding state on the active bond is confined at (but remains above) the chemical potential. This leads to a vanishing transport gap $\Delta_{\rm tr}$. However, this also implies a remarkable constraint in the system; namely, the hole can not delocalize from the active bond into the opposite spectator bond with the same spin orientation.

Another quite important consequence of the orbital flavor mixing is the collapse of the charge polarization on the active bond. Whereas in the absence of orbital polarization in scenario (A) there is a pronounced accumulation of a-type charge at site (0,0,1) and of hole density at site (0,0,0) triggered by the JT interaction, one observes an essentially complete collapse of the combined a plus b charge polarization on the active bond in the case of $D = 0.05$ eV [see Figs. 20(b) and 20(c)].

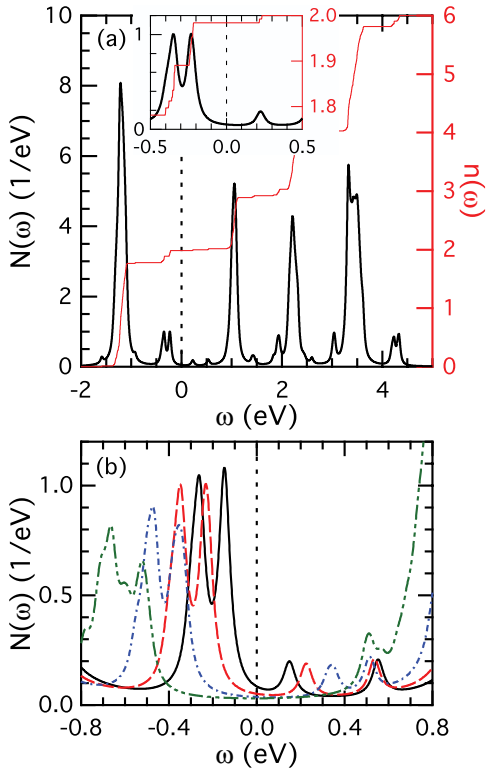

FIG. 21. (Color online) (a) Total DOS $N(\omega)$ (left scale) and average electron filling $n(\omega)$ (right scale) in the dilute well-annealed CG phase at hole doping $x = \frac{1}{64}$, obtained using an $8 \times 8 \times 8$ cluster. The inset shows $N(\omega)$ near the Fermi energy $\omega = 0$. Calculation includes the LR Coulomb interaction $V_{ee} = 0.2$ eV. (b) Dependence of DOS $N(\omega)$ of defect states and Coulomb gap near the Fermi energy $\omega = 0$ on increasing strength of LR Coulomb interaction: $V_{ee} = 0$ (solid line, black), 0.2 eV (dashed line, red), 0.5 eV (dashed-dotted line, blue), 1.0 eV (dashed-double-dotted line, dark green). For increasing strength of V_{ee}, the features in $N(\omega)$ move away from the Fermi energy $\omega = 0$. Other parameters as in set B in Table I and $D = 0$.

D. Role of long-range Coulomb interaction

Next, we turn to the effects of the LR Coulomb interaction in presence of defect states. In insulators, the Coulomb interaction is screened by the dielectric constant ε_0 of the system; yet, the interaction keeps its $\sim 1/\varepsilon_0 r$ LR character. Here, ε_0 represents the background dielectric screening due to the "core" electrons. These are in our case all electrons apart from those of t_{2g} type. The screening arising from t_{2g} electrons, which is for instance essential for the MIT, is explicitly included in the Hamiltonian of the system.

In the next scenario (C), the LR Coulomb interaction (2.20) is taken into account and parametrized via V_{ee} (instead of ε_0), while the orbital polarization is neglected ($D = 0$), as in scenario (A). The DOS is displayed in Figs. 21(a) and 21(b). Its comparison with Fig. 19(a) shows that the LR Coulomb interaction has no significant effect on the ionic multiplet structure, as one might expect. There is, however, a significant change in the size of the energetic splittings between the different defect states in the vicinity of the chemical potential, as one can see from the insets in Figs. 19(a) and 21(a). The

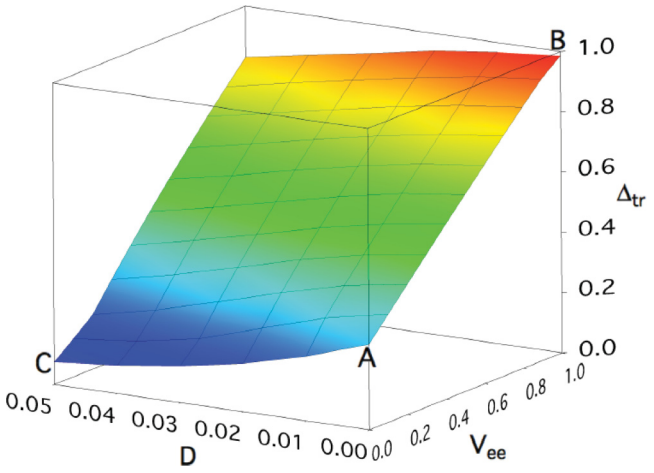

FIG. 22. (Color online) Transport gap Δ_{tr} in the well-annealed CG-AO phase with doping concentration $x = \frac{1}{64}$ as a function of electron-electron interaction coupling V_{ee} and orbital-polarization strength D. Results obtained for an $8 \times 8 \times 8$ cluster with the parameters as in set B of Table I.

fine structure of the levels is here basically as in Figs. 19(c) and 19(d). The peaks in the inset stem from the occupied $\{(c\downarrow),(b\downarrow)\}$ orbitals at the spectator sites as well as from the $(a\downarrow)$ bonding/antibonding levels at the active bond. The main effects of the nonlocal LR electron-electron Coulomb interaction are (i) to enlarge the bonding-antibonding splitting and (ii) to increase the polarity of the active bond.

The transport gap Δ_{tr} opens between the topmost occupied $|c\downarrow b\downarrow\rangle$ states on the spectator site and the unoccupied $|a\downarrow\rangle$ antibonding state on the active bond. Figure 21(b) shows that it increases almost linearly with increasing LR electron-electron interaction $0 < V_{ee} < 1.0$ eV. Indeed, this dependence of Δ_{tr} on V_{ee} is summarized in Fig. 22. The line A-B shows the evolution of Δ_{tr} with the increasing value of V_{ee} for vanishing polarization field $D = 0$. In the absence of nonlocal electron-electron Coulomb interaction, the origin of the gap is the bonding-antibonding splitting due to the kinetic energy gain of the single a electron on the active bond. With increasing V_{ee}, the charge polarization of the bond grows and the kinetic energy is suppressed. At large V_{ee}, the gap Δ_{tr} is determined by the nonlocal Coulomb interactions, i.e., essentially by the nearest- and further-neighbor ones. The increase of Δ_{tr} along the line A-B in Fig. 22 may be approximated in terms of the electron-electron interaction parameter V_{ee}, the hopping integral t, and the JT coupling V_{JT} as follows:

$$\Delta_{tr} \approx \sqrt{(V_{ee}/2 + V_{JT})^2 + t^2} + V_{ee}/2 + V_{JT}. \qquad (5.7)$$

We emphasize that, in these systems, the Coulomb gap in the defect states is a consequence of the complex structure of the defects in combination with the electron-electron interactions. We note that this mechanism is distinct from the disorder-induced Coulomb gap of Shklovskii and Efros.[96] We have already seen that the doped holes in the dilute doping regime have no effect on the multiplet splitting away from the defects. On the other hand, on general grounds we would expect that the present Coulomb gap in the defect band is overestimated within the HF approximation, and will be reduced by dielectric screening, i.e., obtained by

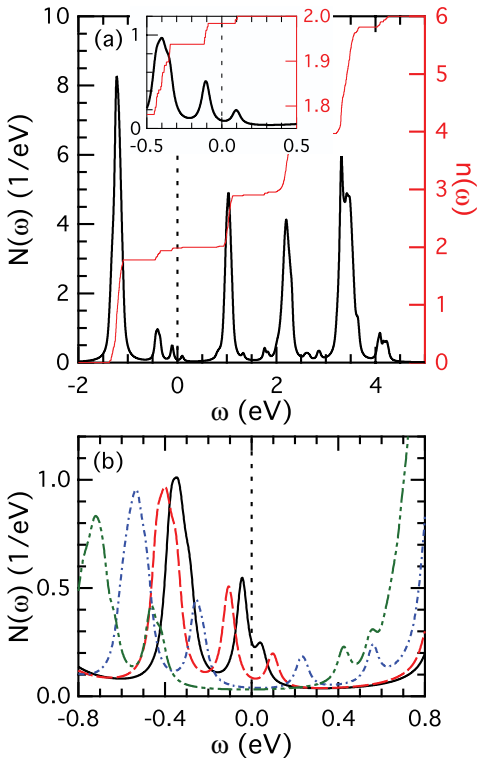

FIG. 23. (Color online) (a) Total DOS $N(\omega)$ (left scale) and average electron filling $n(\omega)$ (right scale) in the dilute well-annealed CG phase with $x = \frac{1}{64}$, as obtained using an $8 \times 8 \times 8$ cluster for finite LR Coulomb interaction $V_{ee} = 0.2$ eV. The inset shows $N(\omega)$ near the Fermi energy $\omega = 0$. (b) DOS $N(\omega)$ of defect states and Coulomb gap near the Fermi energy $\omega = 0$ for increasing strength of LR Coulomb interaction: $V_{ee} = 0$ (solid line, black), 0.2 eV (dashed line, red), 0.5 eV (dashed-dotted line, blue), 1.0 eV (dashed-double-dotted line, dark green). For increasing strength of V_{ee}, the features in $N(\omega)$ move away from the Fermi energy $\omega = 0$. Other parameters as in set B in Table I and $D = 0.05$ eV.

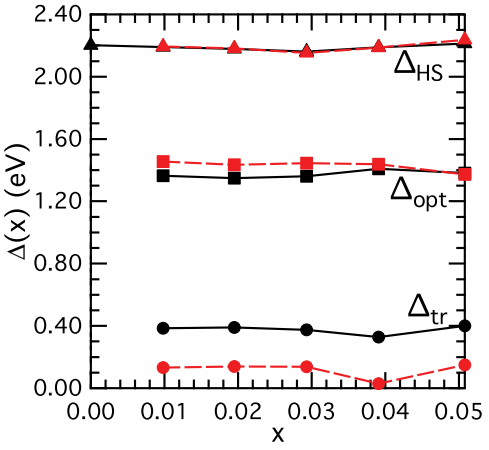

FIG. 24. (Color online) Three characteristic gaps in the spectra for increasing doping x: the Mott gap Δ_{HS} [Eq. (5.2)] deduced from the energy of the HS transitions (triangles), the optical gap Δ_{opt} between the defect states and the HS UHB (squares), and the transport gap Δ_{tr} within the defect states (circles), determined from the flat region in $n(\omega)$ at $\omega = 0$. The three gaps are obtained for the dilute well-annealed doped CG phase using an $8 \times 8 \times 8$ cluster, and for two values of D: $D = 0$ (solid lines, black) and $D = 0.05$ eV (dashed lines, red). Parameters as in set B in Table I and $V_{ee} = 0.2$ eV.

a many-body treatment beyond the HF approach. We shall see next that already the inclusion of orbital polarization gives rise to a substantial screening and reduction of the Coulomb gap.

Finally, we consider scenario (D), which includes both LR electron-electron Coulomb interaction and orbital-polarization effects in the vicinity of the defects. The DOS is displayed in Figs. 23(a) and 23(b). Comparison of the insets in Figs. 23(a) and 21(a) shows the strong reduction of Δ_{tr} in the present case of $D = 0.05$ eV from the value found with $D = 0$. Similarly, Figs. 23(b) and 21(b) make apparent the strong reduction of the gap at $D = 0.05$ eV not only for $V_{ee} = 0$, but also for larger values of V_{ee}.

To summarize, the central observations concerning the transport gap are (i) the decrease of Δ_{tr} with increasing polarization D, and (ii) the increase of Δ_{tr} with increasing LR electron-electron Coulomb interaction strength V_{ee}. These findings are summarized in Fig. 22. The strong impact of the orbital-polarization D term on Δ_{tr} is seen between the A and C points, where the transport gap is reduced by a factor ~ 3 when D increases from 0 to 0.05 eV. This strong suppression of the transport gap change found here for relatively weak polarization interaction D is consistent with fast orbital rotation induced by this term, presented in Sec. III.

VI. DISCUSSION

A. Gaps in the electronic structure

In our HF study we have encountered three fundamental energy scales typical of doped MH insulators. They are displayed in Fig. 24 for the dilute doping regime $x \leqslant 0.05$ investigated here. In decreasing-size order, these energies represent (i) the Mott gap computed as the energy of the HS charge transitions [Eq. (5.2)], (ii) the optical gap Δ_{opt} relevant for the in-gap absorption, which opens between the occupied (unoccupied) defect states inside the MH gap and the unoccupied (occupied) states of the HS part of the UHB (the LHB), and (iii) the lowest-energy excitation gap within the defect states Δ_{tr} [Eq. (5.7)] of relevance for transport. The reported data are obtained for a finite value of the LR Coulomb interaction strength $V_{ee} = 0.2$ eV, and for two different values of the orbital-polarization parameter D, corresponding to scenarios (C) and (D). Note that the gaps Δ_{HS} and Δ_{opt} in Fig. 24 are inferred from the peak positions in the DOS and correspond to the absorption maxima and not to the onset of the absorption.

It is evident that only Δ_{tr} is significantly affected by the orbital-polarization term (Fig. 22). We note here that while the screening of electronic interactions is generally obtained by many-body perturbation theory beyond the HF approximation, for example, by resummation in random phase approximation, the screening of Coulomb interactions at defects is already, to a large extent, contained on the Hartree level and taken care of by charge and orbital relaxation effects around the defects.

This explains why finite orbital polarization D leads to such a strong reduction of the transport gap.

These characteristic scales may be compared with the experimental data[4] for the doping dependence of the optical absorption spectra for $Y_{1-x}Ca_xVO_3$ and $La_{1-x}Sr_xVO_3$. They reveal HS Mott transition energies Δ_{HS} of about 2.2 and 1.8 eV, respectively. The Mott-gap energy is essentially independent of doping, as found in the present HF approach. Only close to the MIT, the intensity of the MH absorption fades away. The most remarkable feature in optical spectroscopy is the appearance of an in-gap absorption related to defect states: the intensity of this absorption grows with doping. The characteristic energy of the in-gap absorption Δ_{opt} (read off at the peak positions) is independent of doping in the dilute limit.

At higher defect concentrations, which go beyond the present model calculations designed for the dilute limit, i.e., for $x < 0.05$, the energy of the absorption peak decreases and eventually collapses for doping concentration approaching the MIT. For example, in the case of $Y_{1-x}Ca_xVO_3$, $\Delta_{opt} \sim 1.2$ eV up to $x = 0.10$.[4] In $La_{1-x}Sr_xVO_3$, this absorption is centered at about 0.80 eV for $x < 0.10$, while the in-gap absorption peak shifts to ~0.3 eV at the doping concentration $x = 0.168$, i.e., close to the MIT.[4] In the high-concentration regime, it will be important to include the dielectric screening due to the doped holes.

Activated transport in $La_{1-x}Sr_xVO_3$ has been reported first by Dougier and Hagenmuller,[97] who observed an activation energy $\Delta_{tr} \sim 80$ meV at $x \simeq 0.05$ doping. Transport in these systems has been extensively discussed by Mott[98] and identified as Anderson type, i.e., controlled by defects. For $Y_{1-x}Ca_xVO_3$, activated behavior of the resistivity was reported for the Ca-doping range $x < 0.3$.[1,5,99] In particular, Sage *et al.*[5] reported the activation energies $E_a = 0.124, 0.106$, and 0.064 eV at doping $x = 0.1$, 0.2, and 0.3, respectively. The values for Δ_{tr} in Fig. 24 are of similar size when orbital polarization $D = 0.05$ eV is included. Noticing these qualitative trends, we point out here that a quantitative analysis of the above experimental data will be possible only after extending the present model to the regime of higher doping $x > 0.1$.

B. Orbital density distribution

Spin-orbital order in RVO_3 compounds is typically discussed by considering only the subspace of a and b orbitals.[19,75] While such a simplified picture may be sufficient for the undoped compounds, it becomes questionable when the system is doped. One important and obvious perturbation mixing the orbitals is the interaction with the dopands. In fact, this interaction triggers the orbital polarization H_{pol}, induced by the polarization constant D in Eq. (2.12). Figure 25 displays the total filling within c and $a + b$ orbitals (defined with respect to the original unrotated orbital basis) as function of doping x. We see that, as expected, the c occupation remains unchanged when the orbital polarization is absent (at $D = 0$), i.e., holes go only into the a and b orbitals. Instead, the situation is reversed for $D = 0.04$ eV and the c occupation is here more strongly reduced than the $a + b$ occupation.

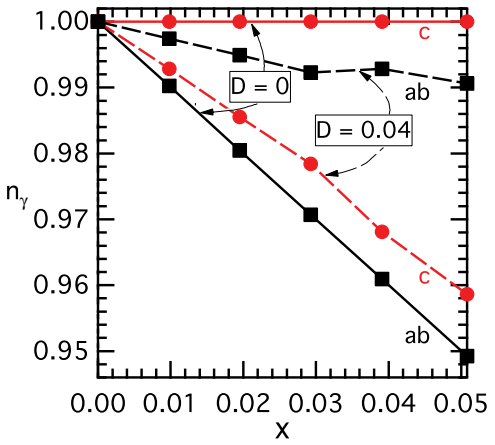

FIG. 25. (Color online) Average total electron filling n_γ in the c orbitals (n_c, circles) and in the $\{a,b\}$ orbital doublet (n_{ab}, squares), as obtained using an $8 \times 8 \times 8$ cluster in the dilute well-annealed CG phase, for increasing doping x and for two values of the orbital-polarization interaction: $D = 0$ (solid lines) and $D = 0.04$ eV (dashed lines). Other parameters as in set B of Table I, and $V_{ee} = 0$.

This, at a first glance, very surprising and counter-intuitive result can be understood by recalling that the lowest (occupied) local states rotate from pure c character at $D = 0$ to a linear combination of c and $\{a,b\}$ at finite D in the vicinity of the defects (see Sec. III). It is important to realize that this rotation involves *all* V neighbors of the defect. Thus, the concentration of V ions affected by the redistribution of electronic density is much larger than the concentration of doped holes; this effect explains the strong change of occupancy seen in Fig. 25.

Considering the strong admixture of a and b orbital character in the rotated c' orbital, one may wonder whether this does not necessarily imply a complete breakdown of any analysis based on a two-flavor description. Such concerns are certainly justified when matrix elements of local orbitals come into play as, for example, in the calculation of the intensities of the transitions investigated in optical or RIXS spectroscopies. We emphasize that in cases where models merely rely on the fact that the rotated c' orbital is the lowest orbital in the t_{2g} sector and is always occupied, qualitative conclusions based on two-flavor models remain valid.

Further insight into the variation of electronic filling in different orbitals at increasing doping x can be gained by inspecting the occupied single-particle states at a spectator site (1,1,0) in the vicinity of a defect at $(\frac{1}{2},\frac{1}{2},\frac{1}{2})$ for finite orbital polarization $D = 0.05$ eV, as displayed in Fig. 26. This figure highlights the formation of bonding and antibonding states on spectator bonds, which involve the $(a\downarrow)$ and $(b\downarrow)$ orbitals as well as the $(c\downarrow)$ orbital (but with a much reduced splitting). An important feature here is that the chemical potential is pinned at the upper edge of the antibonding band. This guarantees that the spectator states are blocked for doped holes!

Another important effect of D is that, with respect to the rotated basis, the hopping matrix no longer conserves flavors, which is the case for the original t_{2g} basis. Therefore, large polarization D leads to a strong mixing of orbitals with different character in the vicinity of defects also via the kinetic energy. One may wonder which mechanism leads to the bonding-antibonding splitting on the spectator bond

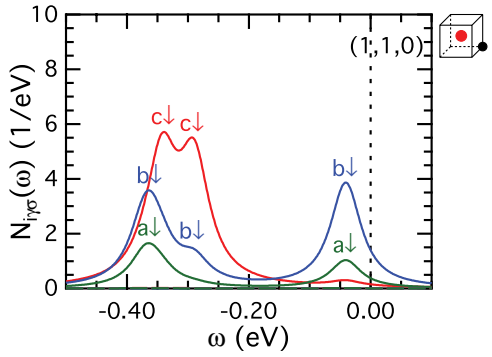

FIG. 26. (Color online) Occupied part of the (spin-orbital)-resolved defect state DOSs $N_{i\alpha\sigma}(\omega)$ for orbital α and spin σ at the atom (1,1,0) which belongs to undoped (*spectator*) bond, as in Fig. 20(d), obtained in the dilute well-annealed doped CG phase ($x = \frac{1}{64}$) using an $8 \times 8 \times 8$ cluster. Parameters as in set B of Table I, $D = 0.05$ eV, and $V_{ee} = 0$.

although both states are occupied such that there is no evident energy gain as, for instance, in the case of the JT splitting or the Peierls distortion. Here, we observe that the splitting is induced by the orbital rotation (at finite D) and the appearance of the off-diagonal hopping processes along the (vertical) c axis. Remarkably, even for the rotated c orbital, hopping along the c axis is now possible, as one can see from a small splitting of the DOS for c electrons in Fig. 26.

VII. SUMMARY AND CONCLUSIONS

Before summarizing, we recall the fundamental problem in strongly correlated systems: the typical multiplet splitting of the transition-metal ions can be obtained in the localized limit by a Hartree factorization performed with respect to an optimal local basis set, i.e., a basis with occupation numbers being close to either 1 or 0. That is, the local spin-orbital states should be either occupied or empty: intermediate values for the occupation numbers would signal the breakdown of the Mott gap in the Hartree approximation, which ultimately happens when the kinetic energy increases and dominates over electron localization triggered by the local interactions. The former requirement, however, leads to complications in the vicinity of defects. This follows from a rotation of the occupied orbital states of the V ions due to the local orbital-polarization fields associated with charged defects.

In principle, a local rotation could be specified that removes the off-diagonal polarization terms and defines a new optimal local basis, i.e., again with occupancies either close to 1 or 0, and a fully developed Mott gap. This simple scheme is not applicable when some nonlocal terms are present (as, e.g., the kinetic energy term). Yet, it is important to recognize that the unrestricted Hartree-Fock (HF) (and not Hartree) scheme, i.e., including the relevant off-diagonal contributions from (local and nonlocal) interactions, can be used to determine the Mott-Hubbard split bands in the presence of defects. We have found that this also holds true for the three-flavor case. In particular, we have shown, by comparison with exact diagonalization, that the HF approach provides a surprisingly faithful description not only of the occupied, but also of the unoccupied, higher multiplet states. It is the latter aspect that is particularly surprising here as it is known that the HF approach is designed to describe the occupied states in the best possible way, while for the unoccupied states one expects a considerably poorer description (e.g., electron affinities).

Basic features of the character of wave functions and excitation spectra, which reflect the interplay of strong correlations and the orbital-polarization field D due to a defect, are already well represented by the HF study of a single ion or a bond embedded into the electronic structure of a large cluster reflecting the Mott insulator with spin-orbital order. These studies and their comparison with exact diagonalization allow us to conclude that the HF calculation describes well (i) the effect of the orbital polarization on the wave functions in the three-flavor case, and (ii) the multiplet structure for an atom (Sec. III). A further investigation for an embedded bond (Sec. IV) highlights the interplay of the orbital-polarization field D and the kinetic energy. Comparison of the HF results for partial densities and excitation spectra (i.e., photoemission and inverse photoemission) with exact diagonalization data shows good agreement in the whole D range. An exception are extremely small values of D, where the exact wave function is entangled, a feature that can not be captured within the HF. A particularly good agreement between the HF and exact diagonalization is obtained for the binding energy basically for all values of $U > 2$ eV. The binding energy for the CG phase is found to be much larger than that for the GC phase. This higher binding energy, together with the double-exchange mechanism realized on ferromagnetic bonds, is responsible for the increasing stability of the CG phase on increasing the doping and leads to the experimentally observed magnetic phase transition in $Y_{1-x}Ca_xVO_3$ at very low doping, $x \sim 0.02$.[43]

The description of doped carriers in Mott insulators, such as in the $R_{1-x}A_xVO_3$ compounds (R = Y, La, and A = Ca, Sr, etc.) or in $LaVO_3/SrVO_3$ superlattices,[100] is a computational challenge due to the interplay of strong correlations, defect-induced local deformations of the wave functions, and spin-orbital order. It is evident that to deal with strong correlations and defects, for sufficiently large systems, requires carefully chosen approximations. In this work, we have shown that the unrestricted HF method fulfills all essential requirements. In particular, we have seen that even the unoccupied states at high energy, i.e., those reflecting the multiplet structure of the Mott insulator at orbital degeneracy, are well described in a doped system. The same holds true for the perturbed electronic structure in the vicinity of the charged defects. The HF approach is an efficient scheme which maps the interacting electron problem onto the problem of a single particle moving in a self-consistently determined field of the other electrons. Therefore, it is applicable for large systems, systems with defects, heterostructures, and interfaces. Very relevant for the success of the method in describing Mott insulators are the broken symmetries reflecting the underlying spin-orbital order. Fortunately, the spin-orbital order in $R_{1-x}A_xVO_3$ compounds persists up to the metal-insulator transition, thus, the assumption of spin-orbital order in the unrestricted HF scheme is here fully justified.

Having shown that the HF approach provides a faithful description of excited states of single defects in systems with

broken symmetries, we investigated the electronic structure of an $8 \times 8 \times 8$ cluster for finite defect concentrations in the dilute doping regime. The aim here is to resolve the complex nature of defect states and their manifestation in the excitation spectra. A single A defect, for example, a divalent A ion in $R_{1-x}A_xVO_3$, adds a hole into the t_{2g} shell of V($3d$) states. In the dilute limit, this hole is not freely moving but is pinned by the charge of the defect essentially to a cube of V ions surrounding the defect A in its center.

This study demonstrates that the excitation spectra of the intrinsic, orbital-degenerate Mott insulator are strongly modified by adding defects. We address here only some points relevant for experimental studies. An important observation is that the fundamental excitations, such as the Mott gap and the multiplet energies, are not affected by doping in the dilute regime. The defects generate defect states inside the Mott-Hubbard gap, as observed.[4] Due to the intrinsic doping, the chemical potential lies inside the defect band. The spectral weight of defect states is taken from the LHB. We have argued that the in-gap absorption observed in the optical conductivity experiments performed for several doped vanadate systems can be identified with these states.

Moreover, we observe in the HF excitation spectra for the CG phase a transport gap inside the defect band, which corresponds to the removal of an electron at one defect and the addition at another defect in the neighborhood. In the absence of electron-electron interactions, this gap is essentially determined by a bonding-antibonding splitting resulting from the c-axis kinetic energy of a doped hole confined by the defect. The inclusion of LR Coulomb interactions between electrons $\sim V_{ee}$ leads to an approximately linear increase of the transport gap with V_{ee}. Thus, these interactions promote the transport gap to a Coulomb gap. By combining Coulomb interactions and the mechanism of orbital polarization, we find a reduction of the size of the Coulomb gap. This can be considered as screening in the vicinity of the localized defect, i.e., screening contained already at the HF level.

An important motivation of this work was the study of the three-flavor case, particularly in connection with defects in the RVO_3 perovskites. Usually, spin-orbital order in the perovskite vanadates is discussed in terms of a simplified two-flavor ($\{a,b\}$) model.[43] We have shown here that defects lead indeed to a strong change of occupied orbitals, e.g., the occupied c orbitals, in the vicinity of charged defects due to orbital polarization. Yet, we have also shown that the topmost occupied local orbitals, i.e., the orbitals that are relevant for the doped holes, are mainly of $\{a,b\}$ character as in the two-flavor description. It is this latter observation that leads to the conclusion that the interaction of doped holes and the spin-orbital degrees of freedom are in fact similar in the two models.

Summarizing, the central result of this paper is establishing that the unrestricted HF approach is well designed to describe the electronic structure of charged defects in doped transition-metal oxides with active orbital degrees of freedom, in presence of strong electron correlations. This study provides valuable insights into the changes of the electronic structure in doped Mott-Hubbard systems under doping. While the positions of the Hubbard subbands are not affected by doping, their spectral intensity changes and new defect states occur within the Mott-Hubbard gap. These new states are observed in the optical spectroscopy and their weight increases with doping.

Finally, we remark that the HF approach represents a natural basis for a subsequent many-body perturbative treatment. It should be noted that the unrestricted HF method already provides the Mott-Hubbard gap and the higher-energy multiplet excitations. Thus, the proper many-body treatment would start from a reasonable Slater determinant, which reflects the correlated electronic structure of the spin-orbital ordered Mott insulator. We have shown that the fundamental Mott gap is correctly described by the HF in the framework of the multiband Hubbard model. Therefore, the many-body treatment will hardly affect the Mott-Hubbard gap, yet it may further improve higher multiplets, and it will certainly contribute to the screening of the long-range Coulomb interactions and lead to an extra reduction of the Coulomb gap in the defect states.

ACKNOWLEDGMENTS

We thank R. Frésard for insightful discussions and G. Khaliullin for careful reading of the manuscript. A.A. thanks the Max-Planck-Institut für Festkörperforschung, Stuttgart, for hospitality and financial support. A.M.O. acknowledges support by the Polish National Science Center (NCN) under Project No. 2012/04/A/ST3/00331.

APPENDIX: HARTREE VERSUS HARTREE-FOCK APPROXIMATION AND OPTIMAL BASIS

The remarkable successes of the LDA + U approach[89] in describing the various aspects of the electronic structure of strongly correlated materials,[101–103] including the magnetic order and the MH gaps, suggest that the Hartree (or mean-field) approximation for the electron-electron interactions in the appropriate orbital basis could be sufficient to design an efficient and realistic scheme to determine the electronic structure. This experience, however, is based on undoped systems, where the occupation numbers for the *atomic* orbitals (such as t_{2g} or e_g orbitals at transition-metal ions in the correlated oxides) used in the LDA + U calculations are either close to 1 or close to 0. This latter condition is actually necessary to produce an essentially correct multiplet splitting, i.e., these orbitals are already the properly chosen orbitals to implement the electron interactions in the Hartree scheme. This is always the case in an undoped Mott insulator, which explains the success of the LDA + U approach.[101–103] Note also that the orbital basis is then identical at every site.

However, in a system with defects, the occupied orbitals (here we consider $\downarrow$-spin ones) belong to an orbital basis, which adjusts itself due to the external polarization field [Eq. (2.12)] (see Sec. III). As a result, for an atom one finds new rotated orbitals $\{|\xi_n\rangle\}$, introduced in Sec. III. Similar situation occurs in a bond but in addition the orbitals are then delocalized over two atoms in the CG phase (see Sec. IV). Hence, we write the HF orbitals for $\downarrow$-spin electrons $\{|\xi_n\rangle\}$ as a linear combination of the original t_{2g} orbitals $\{|ia\rangle,|ib\rangle,|ic\rangle\}$

TABLE II. Decomposition of the local orbital basis [Eq. (A1)] onto the original t_{2g} basis given by the elements $|\alpha_{i\gamma}^{(n)}|^2$ [Eq. (A2)] for $\downarrow$-spin electrons, as obtained for an atom (atom, $n = 1,3,5$) and for a bond with two atoms $i = 1,2$ (bond, $n = 1,\ldots,6$) in the CG phase, with $D = 0.05$ eV. Other parameters as in Table I: set A (atom) and set B (bond).

			Bond		
Orbital	γ	Atom	$i = 1$	$i = 2$	Total
ξ_1	c	0.8616	0.0058	0.0058	0.0116
	b	0.0832	0.3100	0.1842	0.4942
	a	0.0552	0.1842	0.3100	0.4942
ξ_2	c		0.4117	0.4117	0.8234
	b		0.0556	0.0326	0.0882
	a		0.0326	0.0556	0.0882
ξ_3	c	0.0032	0.4337	0.4337	0.8674
	b	0.5381	0.0430	0.0232	0.0662
	a	0.4587	0.0232	0.0430	0.0662
ξ_4	c		0.0096	0.0096	0.0192
	b		0.3293	0.1611	0.4904
	a		0.1611	0.3293	0.4904
ξ_5	c	0.1352	0.0786	0.0786	0.1572
	b	0.3787	0.1150	0.3063	0.4213
	a	0.4861	0.3063	0.1150	0.4213
ξ_6	c		0.0605	0.0605	0.1210
	b		0.1470	0.2925	0.4395
	a		0.2925	0.1470	0.4395

[Eq. (2.6)] at site i:

$$|\xi_n\rangle = \sum_i \sum_{\gamma=a}^{c} \alpha_{i\gamma}^{(n)} |i\gamma\rangle \,. \tag{A1}$$

Here, $i = 1$ and $n = 1,3,5$ for an atom, while $i = 1,2$ and $n = 1,\ldots,6$ for a bond along the c axis. As an example, we give in Table II the expansion coefficients

$$\left|\alpha_{i\gamma}^{(n)}\right|^2 \equiv |\langle \xi_n | i\gamma \rangle|^2 \tag{A2}$$

obtained for a representative value of $D = 0.05$ eV. These coefficients were obtained by applying the unrestricted HF approximation as described in Secs. III and IV.

It is important to realize that the Fock terms that stem from interorbital Coulomb interactions between electrons with the same spin play an essential role in optimizing the orbital basis near charge defects. Indeed, the polarization term (2.12) acts as a field and contains onsite interorbital averages $\langle c_{i\alpha\sigma}^{\dagger} c_{i\beta\sigma} \rangle$ with $\alpha \neq \beta$, which are responsible for the orbital rotation and the change of the local basis. By comparing the occupied orbitals for an atom and for a bond in the C-AF phase at finite value of $t = 0.2$ eV (see Table II), one finds that further change of the orthogonal basis occurs at each site due to finite kinetic energy along the FM bond.[104] Note that the orbital labels $\{n\}$ in Table II are assigned to the orbital functions $\{\xi_n\}$ in sequence of their increasing HF energy. The orbitals $|\xi_1\rangle$ and $|\xi_3\rangle$ are occupied for an atom, while for the bond the number of occupied orbitals is doubled and also the orbitals $|\xi_2\rangle$ and $|\xi_4\rangle$ are occupied: they are characterized by similar orbital densities as those in the orbitals $|\xi_1\rangle$ and $|\xi_3\rangle$ for the atom, respectively, but the energies of the latter two orbitals are interchanged in the bond.

The local electron-electron interactions are rotationally invariant,[59] and the Hartree scheme could in principle be applied to any set of locally orthogonal orbitals including the basis of rotated orbitals discussed above. If one could find such a rotated basis with the self-consistently determined orbital occupations being just either 0 or 1, Hartree approximation would be again sufficient as in the LDA + U scheme. Mean fields would then suffice to come quite close to the exact solution (as for a single atom, see Sec. III), and to reproduce the multiplet structure of the UHB. In such a case, Fock terms simply vanish and one can neglect them from the very beginning despite the fact that terms that could drive finite values of the off-diagonal averages are present in the HF Hamiltonian.

Summarizing, we conclude that the off-diagonal Fock elements are essential within the HF scheme and are necessary to arrive at the final optimal orbitals adjusted to the defect states. It is only in this orbital basis that the electronic structure in a Mott insulator faithfully reproduces the multiplet splittings. Therefore, possible extensions of the LDA + U scheme to doped Mott insulators will have to use downfolding procedure[105] to a proper tight-binding model[106] in which full unrestricted HF calculations could be performed. Designing such a scheme which has to go *beyond* the present LDA + U approach[89] is indeed very challenging; it would make it possible to investigate not only doped Mott insulators but also interfaces,[29,52] heterostructures,[100] or other composite materials with defect states in correlated insulators in the future.

[1] M. Kasuya, Y. Tokura, T. Arima, H. Eisaki, and S. Uchida, Phys. Rev. B **47**, 6197 (1993).

[2] S. Miyasaka, T. Okuda, and Y. Tokura, Phys. Rev. Lett. **85**, 5388 (2000).

[3] J. Fujioka, S. Miyasaka, and Y. Tokura, Phys. Rev. B **72**, 024460 (2005).

[4] J. Fujioka, S. Miyasaka, and Y. Tokura, Phys. Rev. Lett. **97**, 196401 (2006); Phys. Rev. B **77**, 144402 (2008).

[5] M. H. Sage, G. R. Blake, and T. T. M. Palstra, Phys. Rev. B **77**, 155121 (2008).

[6] J. Fujioka, T. Yasue, S. Miyasaka, Y. Yamasaki, T. Arima, H. Sagayama, T. Inami, K. Ishii, and Y. Tokura, Phys. Rev. B **82**, 144425 (2010).

[7] M. Uchida, K. Oishi, M. Matsuo, W. Koshibae, Y. Onose, M. Mori, J. Fujioka, S. Miyasaka, S. Maekawa, and Y. Tokura, Phys. Rev. B **83**, 165127 (2011).

[8] J.-Q. Yan, J.-S. Zhou, J. G. Cheng, J. B. Goodenough, Y. Ren, A. Llobet, and R. J. McQueeney, Phys. Rev. B **84**, 214405 (2011).

[9] A. Damascelli, Z. Hussain, and Z.-X. Shen, Rev. Mod. Phys. **75**, 473 (2003).

[10] P. A. Lee, N. Nagaosa, and X.-G. Wen, Rev. Mod. Phys. **78**, 17 (2006).

[11] A. Avella and F. Mancini, Phys. Rev. B **75**, 134518 (2007); J. Phys.: Condens. Matter **19**, 255209 (2007); **21**, 254209 (2009).

[12] M. Ogata and H. Fukuyama, Rep. Prog. Phys. **71**, 1 (2008).

[13] Philip Phillips, Rev. Mod. Phys. **82**, 1719 (2010).

[14]D. J. Scalapino, Rev. Mod. Phys. **84**, 1383 (2012).
[15]M. Imada, A. Fujimori, and Y. Tokura, Rev. Mod. Phys. **70**, 1039 (1998).
[16]Y. Tokura and N. Nagaosa, Science **288**, 5465 (2000).
[17]A. M. Oleś, G. Khaliullin, P. Horsch, and L. F. Feiner, Phys. Rev. B **72**, 214431 (2005).
[18]Takashi Hotta, Rep. Prog. Phys. **69**, 2061 (2006).
[19]G. Khaliullin, P. Horsch, and A. M. Oleś, Phys. Rev. Lett. **86**, 3879 (2001).
[20]J. Sirker and G. Khaliullin, Phys. Rev. B **67**, 100408 (2003).
[21]P. Horsch, G. Khaliullin, and A. M. Oleś, Phys. Rev. Lett. **91**, 257203 (2003).
[22]G. Khaliullin, P. Horsch, and A. M. Oleś, Phys. Rev. B **70**, 195103 (2004).
[23]G. Khaliullin, Prog. Theor. Phys. Suppl. **160**, 155 (2005).
[24]A. M. Oleś, P. Horsch, L. F. Feiner, and G. Khaliullin, Phys. Rev. Lett. **96**, 147205 (2006); W.-L. You, A. M. Oleś, and P. Horsch, Phys. Rev. B **86**, 094412 (2012).
[25]A. M. Oleś, P. Horsch, and G. Khaliullin, Phys. Rev. B **75**, 184434 (2007).
[26]P. Horsch, A. M. Oleś, L. F. Feiner, and G. Khaliullin, Phys. Rev. Lett. **100**, 167205 (2008).
[27]J. Sirker, A. Herzog, A. M. Oleś, and P. Horsch, Phys. Rev. Lett. **101**, 157204 (2008); A. Herzog, P. Horsch, A. M. Oleś, and J. Sirker, Phys. Rev. B **83**, 245130 (2011).
[28]A. M. Oleś, J. Phys.: Condens. Matter **24**, 313201 (2012).
[29]H. Y. Hwang, Y. Iwasa, M. Kawasaki, B. Keimer, N. Nagaosa, and Y. Tokura, Nat. Mater. **11**, 103 (2012).
[30]J. Zaanen and A. M. Oleś, Phys. Rev. B **48**, 7197 (1993).
[31]G. Khaliullin and S. Maekawa, Phys. Rev. Lett. **85**, 3950 (2000); G. Khaliullin, Phys. Rev. B **64**, 212405 (2001).
[32]G. Jackeli and G. Khaliullin, Phys. Rev. Lett. **101**, 216804 (2008).
[33]G. Jackeli and G. Khaliullin, Phys. Rev. Lett. **102**, 017205 (2009); J. Chaloupka, G. Jackeli, and G. Khaliullin, *ibid.* **105**, 027204 (2010).
[34]J. Kim, D. Casa, M. H. Upton, T. Gog, Y.-J. Kim, J. F. Mitchell, M. van Veenendaal, M. Daghofer, J. van den Brink, G. Khaliullin, and B. J. Kim, Phys. Rev. Lett. **108**, 177003 (2012).
[35]C. Y. Chen, R. J. Birgeneau, M. A. Kastner, N. W. Preyer, and T. Thio, Phys. Rev. B **43**, 392 (1991).
[36]We call the phase with G-type antiferromagnetic (Néel) order accompanied by C-type orbital order (with the same occupied orbitals along the c cubic axis and alternating orbitals within the ab plane) a GC phase, and the phase with C-type antiferromagnetic order (ferromagnetic spin order along the c cubic axis and staggered moments within the ab plane) and staggered orbitals in all three directions a CG phase.
[37]P. G. de Gennes, Phys. Rev. **118**, 141 (1960).
[38]J. van den Brink and D. Khomskii, Phys. Rev. Lett. **82**, 1016 (1999).
[39]P. Horsch, J. Jaklič, and F. Mack, Phys. Rev. B **59**, R14149 (1999).
[40]T. L. van den Berg, P. Lombardo, R. O. Kuzian, and R. Hayn, Phys. Rev. B **86**, 235114 (2012).
[41]A. M. Oleś and G. Khaliullin, Phys. Rev. B **84**, 214414 (2011).
[42]The superexchange along the V^{3+}-V^{4+} bonds is given by t^2/J_H processes in contrast to $t^2/(U-3J_H)$ ones in a Mott insulator, where t is the hopping and U and J_H are the intraorbital Coulomb and Hund's exchange elements, similar as in hole-doped manganites. See A. M. Oleś and L. F. Feiner, Phys. Rev. B **65**, 052414 (2002).
[43]P. Horsch and A. M. Oleś, Phys. Rev. B **84**, 064429 (2011).
[44]Y. Matiks, P. Horsch, R. K. Kremer, B. Keimer, and A. V. Boris, Phys. Rev. Lett. **103**, 187401 (2009).
[45]P. Wróbel and A. M. Oleś, Phys. Rev. Lett. **104**, 206401 (2010); P. Wróbel, R. Eder, and A. M. Oleś, Phys. Rev. B **86**, 064415 (2012).
[46]V. F. Gantmakher, *Electrons and Disorder in Solids* (Clarendon, Oxford, 2005).
[47]T. Mizokawa, D. I. Khomskii, and G. A. Sawatzky, Phys. Rev. B **61**, R3776 (2000).
[48]R. A. Evarestov, S. Piskunov, E. A. Kotomin, and G. Borstel, Phys. Rev. B **67**, 064101 (2003).
[49]W. Chen, G. Khaliullin, and O. P. Sushkov, Phys. Rev. B **80**, 094519 (2009).
[50]J. Carrasco, F. Illas, N. Lopez, E. A. Kotomin, Yu. F. Zhukovskii, R. A. Evarestov, Yu. A. Mastrikov, S. Piskunov, and J. Maier, Phys. Rev. B **73**, 064106 (2006).
[51]I. V. Kondakova, R. O. Kuzian, L. Raymond, R. Hayn, and V. V. Laguta, Phys. Rev. B **79**, 134117 (2009).
[52]N. Pavlenko, T. Kopp, E. Y. Tsymbal, J. Mannhart, and G. A. Sawatzky, Phys. Rev. B **86**, 064431 (2012).
[53]P. Yu and M. Cardona, *Fundamentals of Semiconductors* (Springer, Heidelberg, 1996).
[54]H. J. Queisser and E. E. Haller, Science **281**, 945 (1998).
[55]*Theory of Defects in Semiconductors*, edited by D. A. Drabold and S. K. Estreicher (Springer, Berlin, 2007).
[56]H. Sawada, N. Hamada, K. Terakura, and T. Asada, Phys. Rev. B **53**, 12742 (1996).
[57]I. V. Solovyev, Phys. Rev. B **74**, 054412 (2006); J. Comput. Electron. **10**, 21 (2011).
[58]M. De Raychaudhury, E. Pavarini, and O. K. Andersen, Phys. Rev. Lett. **99**, 126402 (2007).
[59]A. M. Oleś, Phys. Rev. B **28**, 327 (1983).
[60]A. Bourgeois, A. A. Aligia, and M. J. Rozenberg, Phys. Rev. Lett. **102**, 066402 (2009).
[61]M. Daghofer, A. Nicholson, A. Moreo, and E. Dagotto, Phys. Rev. B **81**, 014511 (2010).
[62]G. W. Pratt, Phys. Rev. **102**, 1303 (1956).
[63]T. Mizokawa and A. Fujimori, Phys. Rev. B **51**, 12880 (1995); **53**, R4201 (1996); **54**, 5368 (1996).
[64]H. Weng and K. Terakura, Phys. Rev. B **82**, 115105 (2010).
[65]A. M. Oleś and J. Zaanen, Phys. Rev. B **39**, 9175 (1989).
[66]A. M. Oleś and W. Grzelka, Phys. Rev. B **44**, 9531 (1991); K. Wohlfeld, A. M. Oleś, and G. A. Sawatzky, *ibid.* **75**, 180501 (2007).
[67]B. H. Kim and B. I. Min, Phys. Rev. B **80**, 064416 (2009).
[68]G. Seibold, R. S. Markiewicz, and J. Lorenzana, Phys. Rev. B **83**, 205108 (2011).
[69]I. V. Solovyev, J. Phys.: Condens. Matter **23**, 326002 (2011).
[70]E. Dagotto, T. Hotta, and A. Moreo, Phys. Rep. **344**, 1 (2001); E. Dagotto, New J. Phys. **7**, 67 (2005).
[71]A. Weiße and H. Fehske, New J. Phys. **6**, 158 (2004).
[72]Y. Tokura, Rep. Prog. Phys. **69**, 797 (2006).
[73]L. F. Feiner and A. M. Oleś, Phys. Rev. B **59**, 3295 (1999).
[74]S. Miyasaka, Y. Okimoto, M. Iwama, and Y. Tokura, Phys. Rev. B **68**, 100406 (2003); S. Miyasaka, J. Fujioka, M. Iwama, Y. Okimoto, and Y. Tokura, *ibid.* **73**, 224436 (2006).
[75]Y. Ren, T. T. M. Palstra, D. I. Khomskii, E. Pellegrin, A. A. Nugroho, A. A. Menovsky, and G. A. Sawatzky, Nature (London) **396**, 441 (1998); Y. Ren, T. T. M. Palstra, D. I. Khomskii, A. A.

Nugroho, A. A. Menovsky, and G. A. Sawatzky, Phys. Rev. B **62**, 6577 (2000).

[76]M. Noguchi, A. Nakazawa, S. Oka, T. Arima, Y. Wakabayashi, H. Nakao, and Y. Murakami, Phys. Rev. B **62**, R9271 (2000).

[77]S. Miyasaka, Y. Okimoto, and Y. Tokura, J. Phys. Soc. Jpn. **71**, 2086 (2002).

[78]C. Ulrich, G. Khaliullin, J. Sirker, M. Reehuis, M. Ohl, S. Miyasaka, Y. Tokura, and B. Keimer, Phys. Rev. Lett. **91**, 257202 (2003).

[79]L. D. Tung, A. Ivanov, J. Schefer, M. R. Lees, G. Balakrishnan, and D. McK. Paul, Phys. Rev. B **78**, 054416 (2008).

[80]M. Reehuis, C. Ulrich, P. Pattison, B. Ouladdiaf, M. C. Rheinstädter, M. Ohl, L. P. Regnault, M. Miyasaka, Y. Tokura, and B. Keimer, Phys. Rev. B **73**, 094440 (2006); M. Reehuis, C. Ulrich, K. Prokeš, S. Mat'aš, J. Fujioka, S. Miyasaka, Y. Tokura, and B. Keimer, *ibid.* **83**, 064404 (2011).

[81]J.-S. Zhou, J. B. Goodenough, J.-Q. Yan, and Y. Ren, Phys. Rev. Lett. **99**, 156401 (2007); J.-Q. Yan, J.-S. Zhou, J. B. Goodenough, Y. Ren, J. G. Cheng, S. Chang, J. Zarestky, O. Garlea, A. Llobet, H. D. Zhou, Y. Sui, W. H. Su, and R. J. McQueeney, *ibid.* **99**, 197201 (2007).

[82]D. A. Mazurenko, A. A. Nugroho, T. T. M. Palstra, and P. H. M. van Loosdrecht, Phys. Rev. Lett. **101**, 245702 (2008).

[83]J.-S. Zhou, J. B. Goodenough, J.-Q. Yan, J.-G. Cheng, K. Matsubayashi, Y. Uwatoko, and Y. Ren, Phys. Rev. B **80**, 224422 (2009).

[84]T. Mizokawa, D. I. Khomskii, and G. A. Sawatzky, Phys. Rev. B **60**, 7309 (1999).

[85]J. S. Griffith, *The Theory of Transition Metal Ions* (Cambridge University Press, Cambridge, 1971).

[86]C. Barreteau, R. Guirado-López, D. Spanjaard, M.-C. Desjonquères, and A. M. Oleś, Phys. Rev. B **61**, 7781 (2000).

[87]C. Barreteau, M.-C. Desjonquères, A. M. Oleś, and D. Spanjaard, Phys. Rev. B **69**, 064432 (2004).

[88]M.-C. Desjonquères, C. Barreteau, G. Autès, and D. Spanjaard, Phys. Rev. B **76**, 024412 (2007).

[89]V. I. Anisimov, J. Zaanen, and O. K. Andersen, Phys. Rev. B **44**, 943 (1991); A. I. Liechtenstein, V. I. Anisimov, and J. Zaanen, *ibid.* **52**, R5467 (1995).

[90]G. Stollhoff, A. M. Oleś, and V. Heine, Phys. Rev. B **41**, 7028 (1990); Phys. Rev. Lett. **76**, 855 (1996).

[91]Using the parameter set B of Table I, one obtains energies per site: $E_{CG} = -2.241$ eV and $E_{GC} = -2.200$ eV. The CG phase has then lower total energy and this situation is realized in $LaVO_3$, where the CG phase is more stable. In contrast, the available experiments have concluded that the GC phase is more stable in YVO_3. This could be easily obtained within the present model by a proper fine tuning of the model parameters. At any rate, on slightly increasing the doping, $x \sim 0.02$, the GC phase destabilizes in $Y_{1-x}Ca_xVO_3$ too in favor of the CG phase. This phase transition was qualitatively discussed in the two-flavor model (Ref. 43), where it has been shown that increasing stability of the CG phase with doping is generic and follows from the double-exchange mechanism (Refs. 37–40).

[92]These excitations are obtained by diagonalizing the onsite Hamiltonian (2.16) in the subspace of three degenerate t_{2g} orbitals filled by $m = 2$ electrons.

[93]H. Eskes, M. B. J. Meinders, and G. A. Sawatzky, Phys. Rev. Lett. **67**, 1035 (1991); M. B. J. Meinders, H. Eskes, and G. A. Sawatzky, Phys. Rev. B **48**, 3916 (1993).

[94]This choice avoids the unphysical regime of $U < 1.8$ eV where the first excitation energy Eq. (2.32) is negative.

[95]H. Eskes and A. M. Oleś, Phys. Rev. Lett. **73**, 1279 (1994); H. Eskes, A. M. Oleś, M. B. J. Meinders, and W. Stephan, Phys. Rev. B **50**, 17980 (1994).

[96]A. L. Efros and B. I. Shklovskii, J. Phys. C: Solid State Phys. **8**, L49 (1975).

[97]P. Dougier and P. Hagenmuller, J. Solid State Chem. **15**, 158 (1975).

[98]N. F. Mott, J. Phys. (France) **50**, 2811 (1989).

[99]F. Cintolesi, P. Ghigna, A. Lascialfari, and G. B. Parravicini, Phys. Chem. Chem. Phys. **5**, 4691 (2003).

[100]U. Lüders, W. C. Sheets, A. David, W. Prellier, and R. Frésard, Phys. Rev. B **80**, 241102(R) (2009).

[101]V. I. Anisimov, F. Aryasetiawan, and A. I. Lichtenstein, J. Phys.: Condens. Matter **9**, 767 (1997).

[102]I. V. Solovyev, Phys. Rev. B **69**, 134403 (2004); J. Phys.: Condens. Matter **20**, 293201 (2008).

[103]M. Imada and T. Miyake, J. Phys. Soc. Jpn. **79**, 112001 (2010).

[104]For AF bonds, the hopping is blocked by double exchange (Refs. 37–40) so this orbital modification by the hopping processes is absent as long and the magnetic order persists, at least locally.

[105]O. K. Andersen and T. Saha-Dasgupta, Phys. Rev. B **62**, R16219 (2000); E. Zurek, O. Jepsen, and O. K. Andersen, Chem. Phys. Chem. **6**, 1934 (2005).

[106]O. Gunnarsson, in *Correlated Electrons: From Models to Materials Modeling and Simulation*, Vol. 2, edited by E. Pavarini, E. Koch, F. Anders, and M. Jarrell (Forschungszentrum Jülich, Jülich, 2012), Chap. 9.